BVRIJK light curves and radial velocity curves
for selected Magellanic Cloud Cepheids ⋆,⋆⋆

Jesper Storm[1], Bruce W. Carney[2], Wolfgang P. Gieren[3], Pascal Fouqué[4,5], Wendy L. Freedman[6], Barry F. Madore[7], and Michael J. Habgood[2]

1 Astrophysikalisches Institut Potsdam, An der Sternwarte 16, D-14482 Potsdam, Germany; e-mail: jstorm@aip.de
2 Univ. of North Carolina at Chapel Hill, Dept. of Physics and Astronomy, Phillips Hall, Chapel Hill, NC-27599-3255, USA;
   e-mail: bruce@physics.unc.edu
3 Universidad de Concepción, Departamento de Física, Casilla 160-C, Concepción, Chile; e-mail: wgieren@coma.cfm.udec.cl
4 Observatoire de Paris, Section de Meudon DESPA F-92195 Meudon Cedex, France
5 European Southern Observatory, Casilla 19001, Santiago 19, Chile; e-mail: pfouque@eso.org
6 The Observatories, Carnegie Institution of Washington, 813 Santa Barbara Street, Pasadena, California 91101, USA;
   e-mail: wendy@ociw.edu
7 California Institute of Technology, IPAC, MC 100-22, Pasadena, California 91125, USA; e-mail: barry@ipac.caltech.edu

Abstract. We present high precision and well sampled *BVRIJK* light curves and radial velocity curves for a sample of five Cepheids in the SMC. In addition we present radial velocity curves for three Cepheids in the LMC. The low metallicity ([Fe/H] ≈ -0.7) SMC stars have been selected for use in a Baade-Wesselink type analysis to constrain the metallicity effect on the Cepheid Period-Luminosity relation. The stars have periods of around 15 days so they are similar to the Cepheids observed by the Extragalactic Distance Scale Key Project on the Hubble Space Telescope. We show that the stars are representative of the SMC Cepheid population at that period and thus will provide a good sample for the proposed analysis. The actual Baade-Wesselink analysis are presented in a companion paper.

Key words. Cepheids – Magellanic Clouds

1. Introduction

Recently Freedman et al. (2001) have concluded the Hubble Space Telescope key project on the Extragalactic Distance Scale. They applied the Cepheid Period-Luminosity relation to Cepheids in distant galaxies to calibrate secondary standard candles which in turn can be used to measure the free Hubble flow in the Universe to an accuracy of better than 10%. This result depends on the distance to the Large Magellanic Cloud, which has been assumed to be $(m - M)_0 = 18.5 \pm 0.1$, and on the assumption that the PL relation is only weakly dependent on metallicity. Many studies in the last decade have tried to resolve both of these issues, but widely differing results keep turning up.

In this paper we present data which will be used for a study of the metallicity effect on the PL relation. The idea is to determine the luminosities of individual, low metallicity ([Fe/H] ≈ -0.7), SMC Cepheids and compare these luminosities to those of solar metallicity Galactic Cepheids of similar period. The low metallicity of the SMC Cepheids combined with the solar metallicity Galactic stars provide a reasonably large range in metallicity to place significant constraints on the effect metallicity has on the PL relation.

The recent calibration of the infrared surface brightness method (Fouqué & Gieren 1997) provides a powerful tool for determining luminosities to individual Cepheids. However, to exploit the full potential of the method accurate optical (*V*-band) and near-IR (*K*-band) light curves, as well as well-sampled and accurate radial velocity curves are needed. In the present paper we present all the observational data which is needed for the analysis. Preliminary analyses and discussions have already been presented in Storm et al. (1998, 1999 and 2000), and in a companion paper (Storm et al. 2003) we present our final surface brightness analysis of the stars and determine the constraints on the metallicity effect on the Cepheid PL relation, and the consequences for the value of the Hubble constant.

Five Cepheids in the south-western part of the SMC about 1 degree from the main body of the galaxy were selected for

---

Table 1. The coordinates of the Cepheids as returned by skycat from the Digital Sky Survey (J2000.0).

Identifier	OGLE ID	RA hh:mm:ss	DEC dd:mm:ss
		SMC	
HV 822	SC2-84516	00:41:55.6	−73:32:25
HV 1328		00:32:54.7	−73:49:20
HV 1333		00:36:03.5	−73:55:58
HV 1335	SC1-00001	00:36:55.4	−73:56:30
HV 1345	SC2-41552	00:40:38.5	−73:13:14
		LMC	
HV 2694	SC16-70661	05:35:32.0	−69:43:22
HV 12797		05:22:24.0	−71:59:19
HV 12198		05:13:26.7	−65:27:05

further study. With this location the stars are representative of the SMC population but not affected by the variable extinction and severe crowding which is found closer to the main body of the SMC. The coordinates for the stars are listed in Table 1. Finding charts can be found in Hodge & Wright (1977). The stars were selected to have periods around 15 days, long enough to avoid overtone pulsators, and to guarantee similarity to Cepheids used for extragalactic distance determination, but still short enough to allow a complete phase coverage with a reasonable number of nights at the telescope. Using a sample of almost equal period stars also allows us to probe the intrinsic width of the instability strip at this period.

In addition to the SMC sample we also observed a few LMC Cepheids of different periods, and for completeness we present the data acquired for these stars here as well.

2. The Optical Photometric Data

2.1. The Observations

The Cepheids were observed with a number of CCD cameras at the Las Campanas, Cerro Tololo and La Silla observatories in Chile as summarized in Table 2. The stars were observed in the *BVR* and *I* bands and the exposure times ranged from 30 secs to a few minutes depending on the instrument sensitivity, the seeing and the transparency of the sky. The seeing was typically in the range 0.9 to 1.4 arcsec and all frames with seeing worse than about 2 arcsec were discarded as crowding effects started to become significant. In all cases the point spread function (PSF) was well sampled by the detector.

2.2. Data reduction

2.2.1. Pre-processing

The CCD frames were bias subtracted using a constant value for the bias level determined from bias exposures. The flat fielding was done using sky flatfields for the large scale structure and dome flatfields for the pixel to pixel variations in case of the Las Campanas data. For the CTIO data, the high read-out speed of the detector (about 15 seconds for a full frame) allowed the exclusive use of sky flatfields for the gain calibration.

The 1989 observing run at Las Campanas was somewhat compromised by significant gain variations of the UV-flooded Texas Instrument CCD during the individual nights. After various experiments we have been reasonably successful in scaling and interpolating the flatfields for each science frame to compensate the effect, but these data are of lower quality than those obtained with the other instruments.

2.2.2. Relative photometry

The relative photometry was determined using the DoPHOT_2.0 package (Schecter et al. 1993). The intermediate photometric system was defined by the CTIO observations from the night Jan.2, 1994 as the CTIO system is close to the standard Landolt (1992) system. Furthermore the seeing and photometric quality was good on this night and seven standard field observations were performed (see below).

For each of the other observing runs transformation to the CTIO system of the form

$$v_{\mathrm{ctio}} = v_{\mathrm{inst}} + \alpha_{vbv} \times (b-v)_{\mathrm{inst}} + \mathrm{const} \qquad (1)$$
$$(b-v)_{\mathrm{ctio}} = \alpha_{bv} \times (b-v)_{\mathrm{inst}} + \mathrm{const} \qquad (2)$$
$$(v-r)_{\mathrm{ctio}} = \alpha_{vr} \times (v-r)_{\mathrm{inst}} + \mathrm{const} \qquad (3)$$
$$(v-i)_{\mathrm{ctio}} = \alpha_{vi} \times (v-i)_{\mathrm{inst}} + \mathrm{const} \qquad (4)$$

were determined. The transformations were first determined for each set of instrument magnitudes *bvri* based on the brightest (lowest estimated error) stars in common with the CTIO data. Typically more than 100 stars in each field were used. The coefficients were then averaged over each observing run giving the values listed in Table 2. The typical RMS for the color terms is of the order 0.02 mag. These averaged coefficients were then used for the next iteration where only the zero points for the individual frames were fitted. The final transformation of the *bvri* sets to the CTIO system was then performed using these zero points and the average transformation coefficients.

2.2.3. Transformation to the standard system

On the night of Jan. 2, 1994 we observed three Landolt (1992) fields. Each field was observed two or three times at different airmass giving a total of 31 *BVRI* measurements of standard stars covering a wide range in color $(-0.3 < (B-V) < 1.9)$ and airmass $(1.1 < X < 1.8)$. Synthetic aperture photometry was performed using the IRAF[1] `noao.digiphot.apphot` package and employing an aperture radius of 18 pixels corresponding to a diaphragm diameter of 14 arc-seconds, which also happens to be very similar to the one employed by Landolt (1992).

The IRAF `photcal` package was used to derive the transformations in the form

$$M = m + \alpha_m \times \mathrm{color} + k_m \times X + c_m \qquad (5)$$

where M refers to standard magnitudes and m to the CTIO instrumental magnitudes, color refers to the instrumental color

---

[1] IRAF is the Image Reduction and Analysis Facility, made available to the astronomical community by the National Optical Astronomy Observatories, which are operated by AURA, Inc., under cooperative agreement with the National Science Foundation.

Table 2. Coefficients for the transformation of the various instrument systems to the CTIO instrument system.

Observing period	Observatory	Instrument (Detector)	α_{vbv}	α_{bv}	α_{vr}	α_{vi}
Nov. 1988	LCO	1m (TI#1)	−0.089	1.168	0.890	0.898
Jul. 1989	CTIO	0.9m (RCA#5)	−0.077	1.177	0.963	0.963
Jul. 1989	CTIO	0.9m (TI#3)	−0.078	1.112	0.933	0.945
Aug. 1989	CTIO	4m (TI#1)	−0.071	1.268	0.943	0.937
Nov. 1989	LCO	1m (TI#2)	−0.089	1.168	0.890	0.898
Dec. 1993	CTIO	0.9m (Tek#2)	0.000	1.000	1.000	1.000
Jan. 1996	ESO	DFOSC (C1W11/4)	0.032	1.227	0.928	1.022
Jul. 1996	ESO	DFOSC (C1W11/4)	0.032	1.227	0.928	1.022
Jul. 1996	ESO	EFOSC-2 (CCD#40)	0.066	1.076	1.023	1.025
Sep. 1996	ESO	DFOSC (C1W11/4)	0.017	1.097	0.939	1.021
Oct. 1996	CTIO	0.9m (Tek#3)	−0.009	0.932	0.989	0.982

Table 3. Coefficients for the transformation of the CTIO instrument system to the Landolt (1992) system.

	B	V	R	I
color	$(b-v)$	$(b-v)$	$(v-r)$	$(v-i)$
α_m	0.007	0.019	0.008	0.006
σ_α	0.006	0.003	0.005	0.003
k_m	−0.249	−0.147	−0.118	−0.059
σ_k	0.013	0.007	0.007	0.009
c_m	−4.913	−4.204	−4.183	−5.013
σ_c	0.018	0.010	0.010	0.012
RMS	0.018	0.012	0.010	0.012

Table 4. Ephemerides adopted for the stars.

Identifier	Period days	$\log_{10}(P)$	Epoch HJD
HV 822	16.7421	1.223810	2447485.9
HV 1328	15.8360	1.199645	2447486.7
HV 1333	16.2935	1.212014	2447491.3
HV 1335	14.3816	1.157807	2450610.6
HV 1345	13.4784	1.129638	2447496.0
HV 2694	6.9363	0.841128	2449349.4
HV 12797	6.82	0.8338	2432000.0
HV 12198	3.5228	0.550573	2432011.6

term ($(b-v)$ or $(v-r)$ or $(v-i)$) as listed in Table 3, k_m is the extinction coefficient for passband m, X is the airmass and c_m is the zero point for passband m.

The values of the coefficients with the estimated errors are listed in Table 3. Note that the CTIO instrument system closely resembles the standard system.

To tie in the instrumental magnitudes from the DoPHOT PSF fitting photometry, m_{PSF}, with the aperture photometry of the standard star observations we determined the aperture corrections for the PSF photometry for each individual field. HV 822 was the only field which was not observed during this night, and it was tied in with the HV 1345 field on the following night using a similar procedure.

In the case of HV 1335 it was necessary to add an offset of $\Delta V = -0.1$ mag to the magnitudes from the Nov. 1989 run to bring the V light curve into agreement with that obtained from the other instruments. This is the only deviation from the transformations given above, and it is justified as some of the frames from this run are likely to suffer from residual systematic errors in the flatfielding. The fact that the other stars agree reasonably well with the measurements from the other runs indicate that the flatfielding for the Nov. 1989 run overall has been quite successful.

2.3. Ephemerides

The periods for the stars were re-derived from the present data by minimizing the dispersion between the points in the V-band light curve. The epoch of maximum V-light was finally determined by shifting the light curve by eye to obtain a good fit.

For HV 1335 we have adopted the values found by Udalski et al. (1999). The adopted ephemerides are listed in Table 4.

2.4. The light curves

The photometry for the stars is given in Table 10-14 together with the photometric errors as returned by DoPHOT. The light curves are plotted in Fig.1 where the different observing runs are indicated by a different symbol. The phases were determined on the basis of the ephemerides from Table 4.

2.5. Comparison with other sources of photometry

Caldwell & Coulson (1984) presented photoelectric photometry for HV 1335. We find excellent agreement with their light curve when we add an offset of +0.07 mag to their V magnitudes. Such an offset is expected as HV 1335 has two faint ($\Delta V \approx 3.5$) companions within a distance of 5 arcsec which will make the aperture photometry (which includes the two companions) brighter by approximately the observed amount.

Laney & Stobie (1994) quote mean V magnitudes for the two stars HV 1328 and HV 1335 but again based on photoelectric measurements so a precise agreement cannot be expected due to contamination within either the object aperture or the sky aperture.

More recently Udalski et al. (1999) (The OGLE SMC Cepheid database) have published CCD-based BVI light curves for three of the stars presented here, namely HV 822, HV 1335 and HV 1345. For each of these stars they have about 10 B-band, 25 V-band, and 150 I-band observations with good phase
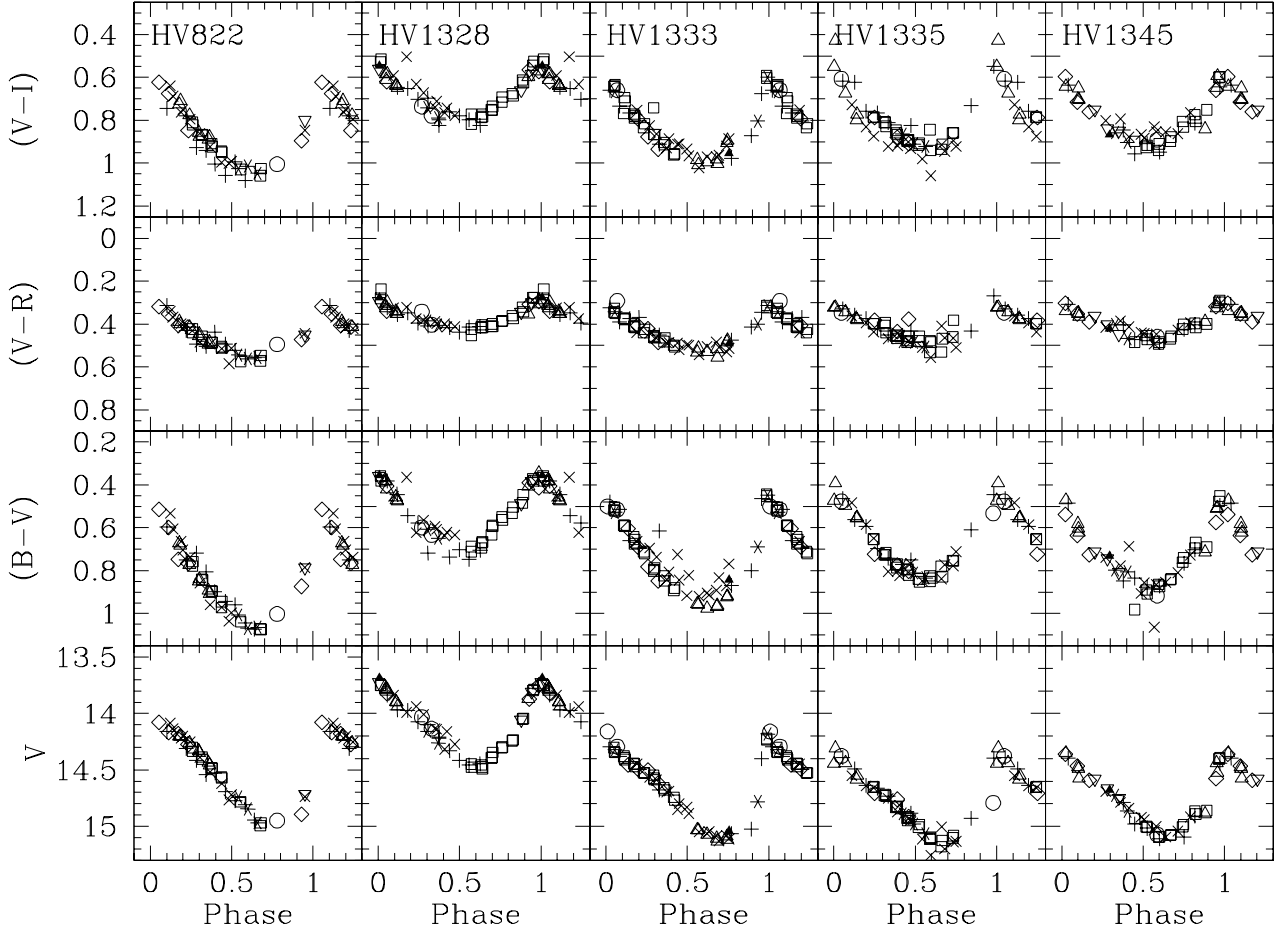
Fig. 1. Light and color curves for the SMC Cepheids. The data are marked in the following way: plusses: LCO 1988, crosses: LCO 1989, open diamonds: CTIO 1989, open squares: CTIO 1993, open inverse triangles: DFOSC Jan. 1996, filled triangles: DFOSC Jul. 1996, open circles: EFOSC-2 Jul. 1996, open triangles: DFOSC Sep. 1996, asterisks: CTIO 1996.

coverage. The agreement with the photometry presented here is good with the zero points agreeing to better than 0.01 mag suggesting that our photometric zero-point is accurate to about 0.01 mag. The only offsets which we have deemed necessary are in the I-band where we have offset their photometry for HV 822 by +0.02 mag and for HV 1335 by +0.03 mag before we determined the mean value.

In Fig. 2 the OGLE V-band light curve for HV 822 has been overplotted on our measurements. The agreement is excellent even though the intensity means of the two data sets differ by 0.05 mag. This difference is, however, mainly due to a different phase coverage especially in the phase range 0.8 to 1.0 where the magnitudes change rapidly and where the light curve exhibits several inflection points.

3. The near-IR data

J and K-band data were acquired for the five SMC stars with a variety of instruments as tabulated in Table 5. As the period of the stars are so long, it only made sense to obtain one or at most two phase points per night. With the limited number of

Table 5. List of observing runs which contributed to the near-IR data set.

Date	Observatory	Instrument
Jan. 1998	ESO, La Silla	2.2m with IRAC-2
Oct. 1998	Las Campanas	1.0m with C40IRC
Dec. 1998	Las Campanas	2.5m with IRCAM
Jan. 1999	Las Campanas	1.0m with C40IRC
Jan. 1999	Las Campanas	2.5m with IRCAM
Jan. 2000	CTIO	1.5m with OSIRIS

stars in the sample it was possible to obtain these data within a short time in parallel to the main observing program (Cepheids in young LMC clusters).

3.1. Data reduction

The observations were made in a five position dither mode enabling a sky frame to be constructed by median filtering these dithered frames. This local sky was subtracted from the
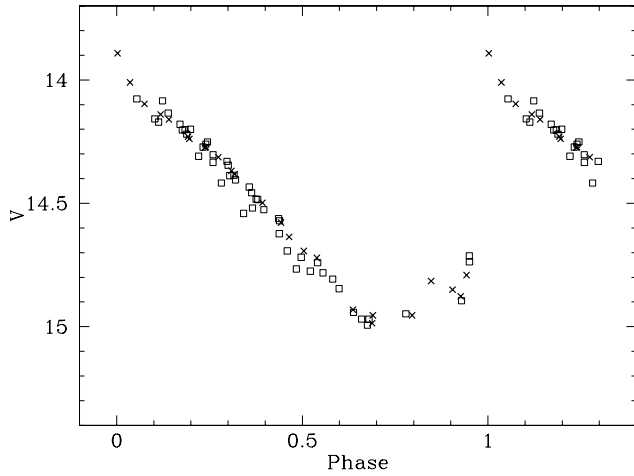
Fig. 2. The *V*-band light curve for HV 822 (open boxes) from our data with the measurements from Udalski et al. (1999) overplotted (crosses).

individual science frames which were then flatfielded by an appropriate flatfield. The flatfield was either made from twilight exposures with an appropriate dark frame subtracted (Las Campanas) or from dome flats where high- and low-light intensity frames with identical exposure time were subtracted from each other (ESO and CTIO).

A linearity correction was applied to the raw frames where appropriate, but all science and calibration frames were obtained with sufficiently low count levels, so the non-linearity does not affect the data (< 1% correction).

3.2. Photometry

The photometry was done using the PSF fitting program DAOPHOT-II (Stetson, 1987) within IRAF. An instrumental photometric system was defined for each field by a set of exposures obtained on a night of good photometric quality. All the frames for the field from the other nights and other instruments were transformed to this system in a manner similar to the process described in a previous section for the optical data. Color terms were determined between the instrumental system and the other instruments on the basis of photometry of stars in the young LMC cluster NGC 2136 with a wide range of $(J-K)$ color. In all cases no significant color term between the instrument systems could be established at the 2% level.

3.3. Calibration to the standard system

During the nights Dec.27 and Dec.28 1998, we observed eight standard stars several times for a total of 21 standard star observations. The stars were all from the list of Persson et al. (1998) and span the color range from $(J-K) = 0.24$ to 0.95. Each observation consisted of four dithered exposures in each of the J and Ks filters. The airmass terms were determined to be similar to the canonical values ($k_J = 0.10$, $k_K = 0.08$) adopted by Persson et al. (1998) so we adopted these values. We also, as expected, did not detect a color term with respect to the Persson

system so we only had to determine the nightly zero points. For the reddest measurements ($(J-K) > 0.45$) we applied the transformation determined by Persson et al. (1998) to transform the data to the CIT system, otherwise the two systems were considered identical.

On the same nights the science fields were also observed, and tertiary reference stars in the fields were tied in with the standard system by applying the offsets determined for the standard stars and correcting for the appropriate airmass term. This was done using the IRAF package `photcal` on synthetic aperture photometry of isolated stars in the fields and using growth curves to take out any variation which might be present due to seeing variations.

The observations from the other nights were offset to the Las Campanas instrument system as described in the previous section and these transformed data were finally transformed to the CIT system using the zero points offsets determined here. The resulting photometry is tabulated in Table 15-19.
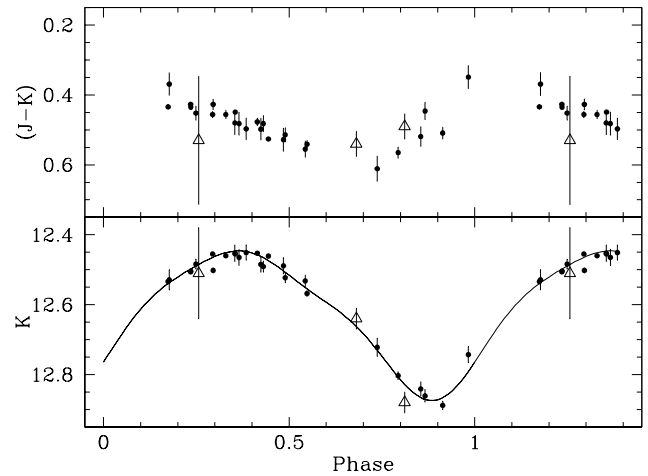
Fig. 3. Near-IR light and color curves for HV 822. Open triangles are from Welch et al. (1987).

3.4. The *K*-band light curve and $(J - K)$ and $(V - K)$ color curves

The main purpose of the near-IR observations is to obtain a well defined $(V - K)$ color curve for each Cepheid which is necessary for the application of the near-IR surface brightness relation to these stars. At the same time we can obtain good J and K light curves and thus a good estimate of the mean J- and K-band magnitudes of the stars, for comparison with the corresponding Cepheid PL relations. The $(J - K)$ color curve can potentially also be used for a Baade-Wesselink type analysis, but for these stars it turns out that the amplitude is very small and thus the photometric uncertainties become very significant. In short, the $(J - K)$ color is a poor (insensitive) temperature indicator for these stars.

We have compared our *K*-band photometry with the measurements by Welch et al. (1987) and find excellent agreement. Their (few) points have been overplotted in the *K*-band light
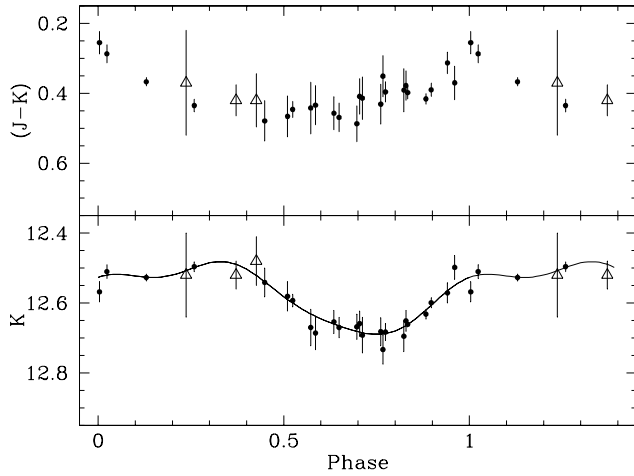
Fig. 4. Near-IR light and color curves for HV 1328. Open triangles are from Welch et al. (1987).
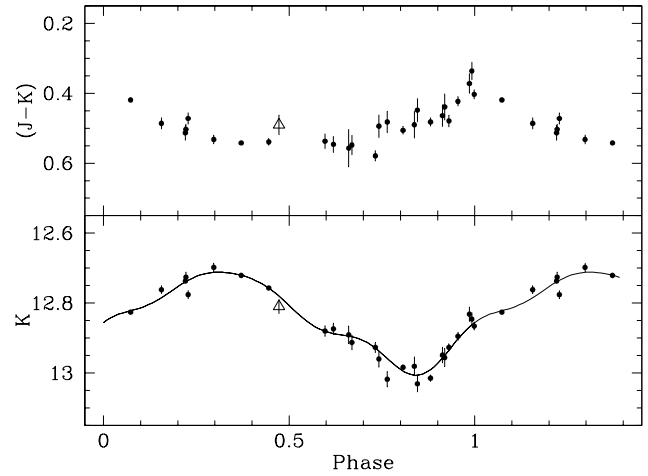
Fig. 7. Near-IR light and color curves for HV 1345. Open triangles are from Welch et al. (1987).
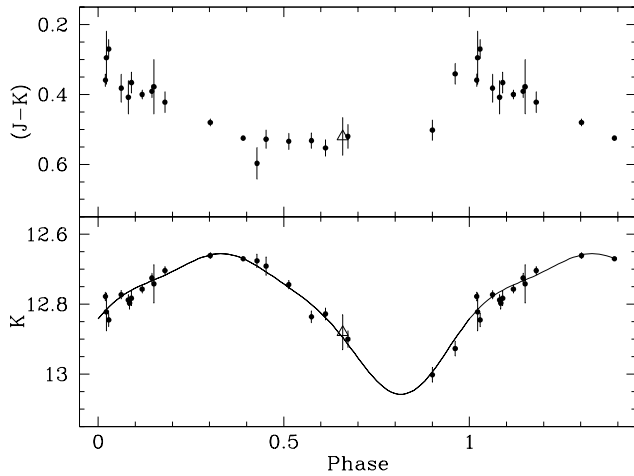
Fig. 5. Near-IR light and color curves for HV 1333. Open triangles are from Welch et al. (1987).
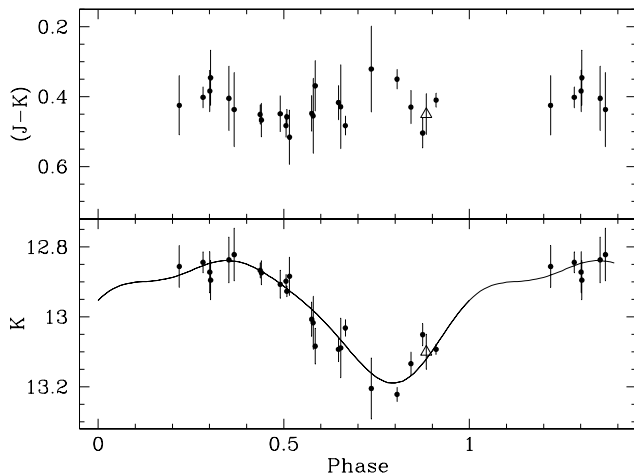
Fig. 6. Near-IR light and color curves for HV 1335. Open triangles are from Welch et al. (1987).

curves and will be used in the determination of the $(V - K)$ color curve.

As the near-IR data were obtained at different times from the V-band observations it is necessary to construct the $(V - K)$ color curve on the basis of the V and K-band light curves, i.e. in phase space. As the observations are not obtained at exactly the same phases, it is necessary to interpolate to obtain the color at a given phase. We decided to do this by fitting a 3rd or 4th order Fourier series to the K-band data and then use this expansion to compute the corresponding K value for each V phase point. The K-band light curve has the lowest amplitude (± 0.15 mag) and is significantly more sinusoidal than the V-band light curve and thus lends itself well to a low order Fourier fit. The low order fits follow the general trend of the light curves rather well and the possible errors introduced from the fit are small. Of course there is an enhanced uncertainty where the phase coverage is poor. We have tried to use different (reasonable) orders for the fits but the resulting Baade-Wesselink results were not affected significantly. The Fourier fit to the data points has been overplotted in Fig.3-7.

To obtain the best possible phase coverage we have combined our V-band data with those of Udalski et al. (1999). No offsets have been applied as we could not determine any offset with a significance of more than 0.01 mag.

The resulting $(V - K)$ color curves are shown in Fig.8 and the photometric values are tabulated in Table 20-24. We note that one point on the $(V - K)$ curve for HV 1335 at phase 0.979 is significant fainter than the neighbouring points. We assume that this is a deviant point and not an indication of a possible phase mismatch. In the Baade-Wesslink analysis we will anyway disregard the phase region from 0.8 to 1.0 as will be discussed in Storm et al. (2003).

4. The Radial Velocities

The radial velocity curves were determined from Echelle spectra obtained with the Las Campanas Observatory 2.5m Du Pont
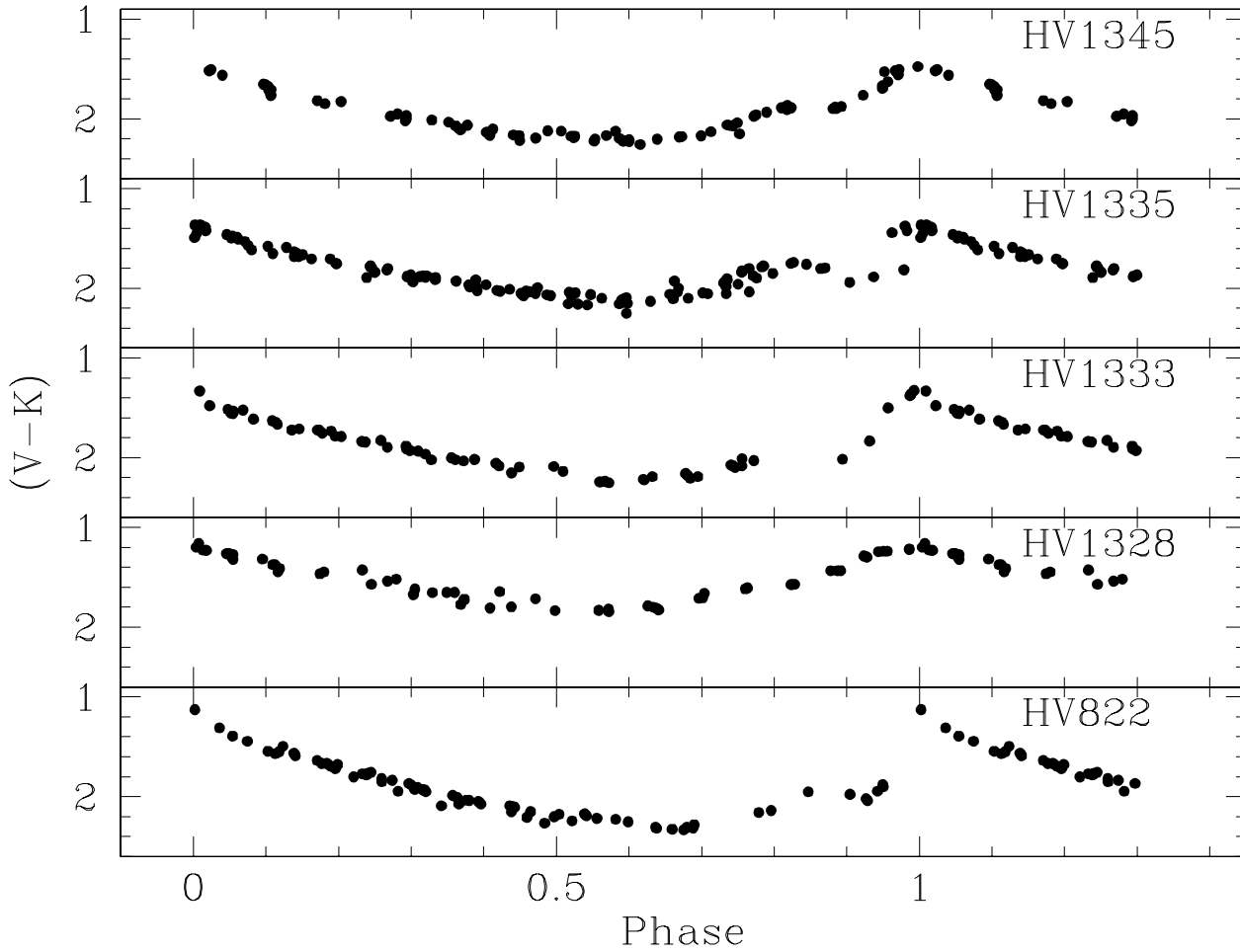
Fig. 8. The $(V - K)$ color curves for the five prime targets.

telescope equipped with the echelle spectrograph and the 2D-Frutti photon counting system.

The spectrograph provides a dispersion of 0.2nm/mm ($\approx$ 0.006nm pix^{-1}) and was used with a slit of 1.5×4 arcsec which transforms into an instrumental profile with a FWHM of approximately 3.5 pixels or 12 km s^{-1} . The spectrograph is very efficient for our purpose, providing typical signal to noise ratios of 10 per resolution element with exposure times ranging from 30 to 60 minutes depending on the brightness of the object.

Additional measurements were secured with the ESO Multi-Mode Instrument (EMMI) mounted at the ESO New Technology Telescope (NTT) at the La Silla Observatory. The red arm of the instrument with a CCD detector (Loral #34) was used with the echelle grating #10 giving a dispersion of 0.24 nm/mm. The efficiency was not quite as high as for the Las Campanas instrument, but similar S/N ratios could be obtained with similar exposure times.

4.1. Observations

The Las Campanas data were obtained during four observing runs in the seasons 1987, 1988, 1989 and 1994 and com-

prise 171 science spectra for the objects described here. The La Silla data were obtained during technical time on one night in October 1992 and a few nights in September 1993 and add an additional 8 velocity measurements. The exact timing of the exposures is listed together with the resulting radial velocities in Table 25 and 26.

Reference Th-Ar exposures of 600 seconds were obtained just before or after each of the scientific exposures. As radial velocity reference we observed the twilight sky as well as the star C349 in 47 Tuc (chart in Chun & Freeman, 1978). 47 Tuc is conveniently located near the SMC so the instrument is pointing in almost the same direction as during the science exposures, thus minimizing any differential flexure and ensuring a minimum overhead of observing time.

4.2. Data Reduction

The echelle spectra were reduced and analysed using IRAF.

The raw data frames were flat-fielded using an average flat-field for each observing run which had the large-scale structure removed and which was normalized. In this way the statistical properties of the data were largely maintained.

The IRAF package `noao.imred.echelle` was used for extracting the orders and for performing the wavelength calibration. Due to limited computing power at the beginning of the project, 10 orders covering the range $\lambda\lambda\,475-555$ nm were used for the first three runs and for the Nov. 1994 run 20 orders covering the range $\lambda\lambda\,417-555$ nm were used. For the NTT data the range $\lambda\lambda\,490-640$ nm was used.

Th-Ar exposures obtained immediately before or immediately after the science exposure with the telescope in the same position were employed for defining the wavelength solution.

The resulting one-dimensional spectra were then fed into the cross-correlation program `XCOR` (for a description see Morse et al. 1991) and for the later runs the related program `XCSAO` (Kurtz et al. 1992) which is part of the `RVSAO` package for IRAF. The algorithms are based on the technique described by Tonry & Davis (1979).

Each echelle order had the continuum fitted and removed by a 5 piece cubic spline and the spectra were rebinned to 2048 bins before the actual cross-correlation.

Extensive tests were performed to find the best wavelength range and to choose the optimal parameters for the filtering of the Fourier spectrum. We found that the best wavelength region was 410-555 nm so these region was used for the last (1994) run, whereas for the earlier runs only the region 475-555 nm was employed. The best filter turned out to ramp up from wavenumber 30 to 40 and taper off from 350 to 400.

In general the twilight sky exposure gave the best cross-correlation peak due to a better signal to noise ratio, and 47 Tuc-C349 was used to determine nightly velocity offsets. For the early data a reference velocity of -21.5 ± 0.2 km s^{-1} was adopted on the basis of the average values from the 1989 run itself and from same epoch CORAVEL data (see Storm et al., 1991). The mean radial velocity for the 1994 run came out as -20.8 ± 0.6 km s^{-1} for 47 Tuc-C349 but this is mostly due to a different selection of wavelength range. Using the same wavelength range as the previous years gave -21.8 km s^{-1}. As we are interested in the best possible relative velocities between the different observing runs we have adopted the value of -21.5 km s^{-1} as the reference velocity and applied nightly shifts to all the nights to bring all the velocities on the same system.

All velocities are referred to the barycenter of the solar system using the facility within `XCSAO` for transferring the observed velocities to this reference frame.

The final velocities were determined from weighted means of the velocities determined for the individual orders. The typical standard deviation for a single order is 3 km s^{-1} and using 10 or 20 orders thus brings down the formal error on the mean to well below 1 km s^{-1}. To this error has to be added the error on the nightly shifts as determined from the observations of C349. This error can be estimated from the standard deviations from the mean and is of the order 1.4 km s^{-1} which should be added quadratically to the internal formal error. Realistic errors can also be estimated from the radial velocity curves themselves (see Fig.9) by determining the spread around a smooth curve. We estimate a standard error of 1.5-2.0 km s^{-1} per observation which is also in good agreement with the computed value.

Table 6. Radial velocities for the reference star 47 Tuc-C349 measured with respect to the twilight sky.

HJD	Rad. vel. km s^{-1}
2449234.7919	−20.6
2449237.7682	−20.3
2449672.5341	−18.3
2449673.5209	−22.2
2449674.5146	−20.8
2449675.5215	−18.5
2449676.5149	−21.6
2449678.5130	−19.9
2449679.5442	−22.0

The velocities are listed in Table 25 and 26 together with the Heliocentric Julian Dates (HJD) at mid-exposure. In Fig.9 the radial velocity curves resulting from these observations and adopting the ephemerides from Table 4 are plotted.
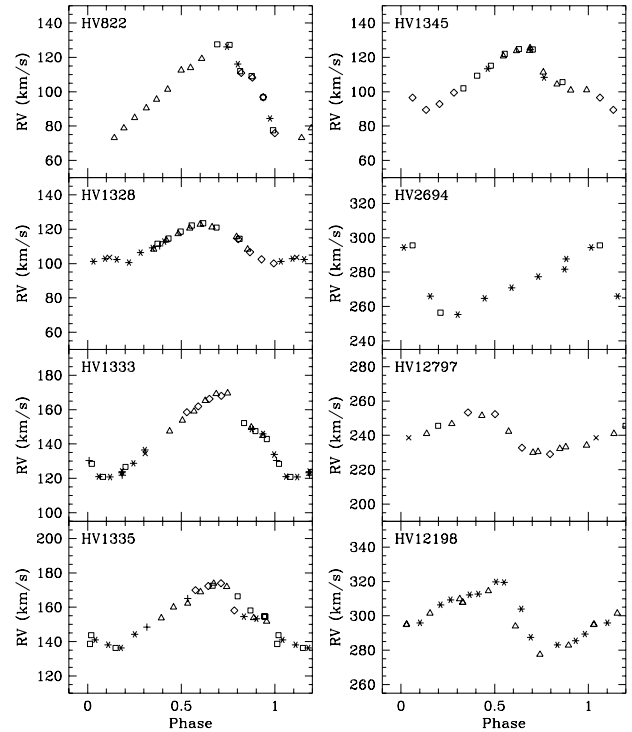
Fig. 9. Radial velocity curves for the cepheids. Note that the radial velocity scale is the same in all the frames. The data are labelled according to the run they were aquired. Open boxes are from 1987, open diamonds 1988, open triangles 1989, asterisks 1994 and crosses and plusses are NTT data from 1992 and 1993 respectively. The three last stars are LMC stars.

A few measurements for HV 821 and HV 883 were obtained as well and they are listed in Table 27.

Table 8. The Fourier coefficients for the V light curves for the SMC Cepheids.

ID	A_1 mag	k	R_{k1}	$\sigma(R_{k1})$	ϕ_{k1}	$\sigma(\phi_{k1})$
HV822	0.41	2	0.31	0.04	4.51	0.12
		3	0.18	0.04	2.58	0.23
		4	0.11	0.03	1.15	0.36
HV1328	0.32	2	0.19	0.02	4.33	0.10
		3	0.14	0.02	1.58	0.14
		4	0.11	0.02	5.28	0.17
HV1333	0.38	2	0.37	0.04	4.88	0.15
		3	0.22	0.05	2.79	0.22
		4	0.26	0.04	1.42	0.24
HV1335	0.34	2	0.30	0.04	4.39	0.18
		3	0.13	0.04	1.35	0.39
		4	0.08	0.04	5.33	0.51
HV1345	0.32	2	0.20	0.04	4.49	0.18
		3	0.18	0.04	1.87	0.22
		4	0.15	0.04	5.50	0.26

Table 9. The Fourier coefficients for the radial velocity curves for the SMC Cepheids.

ID	A_1 $\mathrm{km\,s^{-1}}$	k	R_{k1}	$\sigma(R_{k1})$	ϕ_{k1}	$\sigma(\phi_{k1})$
HV822	27	2	0.25	0.03	2.89	0.14
		3	0.09	0.03	4.62	0.32
		4	0.14	0.03	0.42	0.24
HV1328	11	2	0.19	0.02	4.17	0.12
		3	0.10	0.02	0.14	0.21
		4	0.08	0.02	2.31	0.27
HV1333	22	2	0.13	0.02	2.93	0.18
		3	0.08	0.02	3.63	0.27
		4	0.09	0.02	0.17	0.26
HV1335	16	2	0.06	0.05	3.05	0.86
		3	0.13	0.05	3.23	0.42
		4	0.11	0.05	0.23	0.46
HV1345	15	2	0.18	0.05	5.40	0.28
		3	0.22	0.05	2.54	0.26
		4	0.07	0.05	5.94	0.70

5. Observational Parameters

In Table 7 we summarize the integrated properties of the stars. The magnitudes are all intensity magnitude averages. To assure the best possible phase coverage and optimal definition of the mean magnitudes we have performed the V and I averages over the data presented here combined with the Udalski et al. (1999) data for HV 822, HV 1335, and HV 1345, and the Caldwell & Coulson (1984) data, offset by +0.07 mag in V, for HV 1335. The reddening insensitive Wesenheit index, $\langle W \rangle$, defined as $\langle W \rangle = \langle V \rangle - 2.51(\langle V \rangle - \angle I)$ where sharp brackets indicates intensity averages, has been tabulated as well.

We have also computed the Fourier parameters R_{21} - R_{41} and ϕ_{21} - ϕ_{41} (as defined by Petersen (1986)) for the Cepheids based on the V light curves using $N = 4$, i.e. four components. The resulting parameters are tabulated in Table 8 together with the associated error estimates. The semi-amplitudes for the first (A_1) order are also tabulated. Table 9 contains the same parameters but derived for the radial velocity curves and following the convention from Simon (1988) where the radial velocity coef-
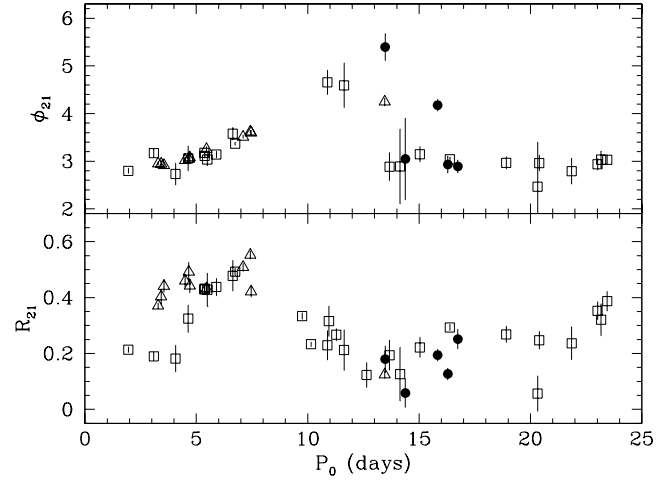
Fig. 10. The radial velocity Fourier parameters for our program stars (filled circles), a solar metallicity galactic sample (open squares), and the low metallicity galactic sample of Pont et al. (2001) (open triangles).

ficients are based on a sine series, which means that the phases are shifted by $\pi/2$ with respect to the cosine series used for the photometric data.

The photometric amplitude ratios R_{21} are in good agreement with the values found by Udalski et al. (1999) for their large sample of SMC stars.

Pont et al. (2001) have obtained accurate radial velocity curves for a sample of Galactic cepheids at relatively large Galactocentric distances with expected lower than solar metallicities. They find weak evidence that the ϕ_{21} parameter is metallicity sensitive for periods longer than about 12 days as the star HW Pup exhibits a significantly larger ϕ_{21} than that found for solar metallicity Cepheids. HW Pup with a period of 13.5 days is indeed metal-poor, with [Fe/H] $= -0.29$ according to Andrievsky et al. (2002) and -0.51 according to de Almeida (priv. comm.).

To further investigate this possibility we have overplotted the data from Pont et al. (2001) in Fig.10 with our data and data from a sample of nearby galactic stars with good radial velocity curves (see the companion paper Storm et al. 2003). We see that a couple of our stars exhibit an even higher value of ϕ_{21} than Pont et al. (2001) found for HW Pup. However, we also have three SMC stars which are in good agreement with the supposedly solar metallicity galactic sample. A clarification of this question will have to await individual spectroscopic metallicities for these stars and possibly also a larger sample.

Acknowledgements

Table 7. Intensity mean magnitudes and colors based on the combined datasets for each star in the sample.

ID	$\langle V \rangle$	$\langle B \rangle - \langle V \rangle$	$\langle V \rangle - \langle R \rangle$	$\langle V \rangle - \langle I \rangle$	$\langle V \rangle - \langle K \rangle$	$\langle J \rangle - \langle K \rangle$	$\langle W \rangle$
HV822	14.523	0.769	0.409	0.861	1.903	0.482	12.362
HV1328	14.116	0.566	0.364	0.678	1.538	0.407	12.413
HV1333	14.707	0.712	0.432	0.839	1.905	0.472	12.601
HV1335	14.808	0.648	0.440	0.798	1.823	0.419	12.805
HV1345	14.763	0.694	0.397	0.800	1.924	0.499	12.756

References

Andrievsky, S.M., Kovtyukh, V.V., Luck, R. E., Lépine, J.R.D., Maciel, W.J., & Beletsky, Yu. V.; 2002, A&A, 392, 491.

Caldwell, J.A.R., and Coulson, I.M.; 1984, SAAO Circ., 8, 1

Chun, M.S., & Freeman, K.C.; 1978, AJ, 83, 376.

Freedman, W.L., Madore, B.F., Gibson, B.K., et al.; 2001, ApJ, 553, 47.

Fouqué, P., & Gieren, W.P, 1997, A&A, 320, 799.

Hodge, P.W., & Wright, F.W.; 1977, "The Small Magellanic Cloud", Univ. of Washington Press, Seattle

Kurtz, M.J., Mink, D.J., Wyatt, W.F., et al.; 1992, in: Worral, D.M., Biemesderfer, C., & Barnes, J. (eds), PASPC, 25, 432

Landolt, A.U.; 1992, AJ, 104, 340.

Laney, C.D., & Stobie, R.S.; 1994, MNRAS, 266, 441.

Morse, J.A., Mathieu, R.D., & Levine, S.E.; 1991, AJ, 101, 1495.

Persson, S.E., Murphy, D.C., Krzeminski, W., Roth, M., & Rieke, M.J.; 1998, AJ, 116, 2475.

Petersen, J.O.; 1986, A&A, 170, 59.

Pont, F., Kienzle, F., Gieren, W., & Fouqué, P.; 2001, A&A, 376, 892.

Schecter, P.L., Mateo, M., & Saha, A.; 1993, PASP, 105, 1342.

Simon, N.R.; in "Pulsation and Mass Loss in Stars", eds. R. Stalio, L.A. Willson, Kluwer, Dordrecht, 1988, Astrophys. & Space Sci. Lib., 148, 27

Stetson, P.B.; 1987, PASP, 99, 191.

Storm, J., Carney, B.W., Freedman, W.L., & Madore, B.F.; 1991, PASP, 103, 261.

Storm, J., Carney, B.W., & Fry, A.M.; in "Views on Distance Indicators", eds. M. Arnaboldi, F. Capuot, & A. Rifatto, 1998, Mem. Soc. Ast. It., 69, 79

Storm, J., Carney, B.W., & Fry, A.M.; in "Harmonizing Cosmic Distance Scales in a Post-HIPPARCOS Era", eds. D. Egret, & A. Heck , 1999, ASP. Conf. Series, 167, 320

Storm, J., Carney, B.W., Gieren, W.P., Fouqué, P., & Fry, A.M.; in "The Impact of Large-Scale Surveys on Pulsating Star Research", eds. L. Szabados, & D. Kurtz, 2000, ASP Conf. Series, 203, 145

Storm, J., Carney, B.W., Gieren, W.P., Fry, A.M., Latham, D.W., & Fouqué, P.; 2003, A&A, Submitted, .

Tonry, J.L., & Davis, M.; 1979, AJ, 84, 1511.

Udalski, A., Soszyński, I., Szymański, M., et al.; 1999, Acta Astr., 49, 437.

Welch, D.L., McLaren, R.A., Madore, B.F., & McAlary, C.W.; 1987, ApJ, 162, 1987.

Table 10. Photometric values for HV 822.

HJD - 2400000. days	Phase	V mag	σ_V mag	$(B-V)$ mag	$\sigma_{(B-V)}$ mag	$(V-R)$ mag	$\sigma_{(V-R)}$ mag	$(V-I)$ mag	$\sigma_{(V-I)}$ mag
47487.62381	0.103	14.158	0.023	0.596	0.029	0.313	0.030	0.746	0.033
47489.59791	0.221	14.309	0.020	0.749	0.029	0.431	0.023	0.778	0.021
47490.62079	0.282	14.418	0.022	0.718	0.030	0.495	0.025	0.928	0.026
47491.62283	0.342	14.541	0.026	0.805	0.032	0.504	0.040	0.940	0.031
47492.53321	0.396	14.526	0.016	0.898	0.023	0.437	0.035	1.004	0.019
47493.59359	0.460	14.693	0.036	0.944	0.044	0.495	0.051	1.058	0.037
47494.63244	0.522	14.775	0.023	0.959	0.029	0.524	0.024	0.993	0.024
47495.63865	0.582	14.807	0.022	1.045	0.031	0.549	0.027	1.080	0.032
47496.58381	0.638	14.942	0.017	1.073	0.023	0.557	0.021	—	—
47735.83864	0.929	14.895	0.012	0.873	0.020	0.473	0.011	0.895	0.014
47737.93934	0.054	14.077	0.007	0.514	0.011	0.319	0.011	0.622	0.010
47738.92064	0.113	14.171	0.012	0.599	0.017	0.354	0.016	0.677	0.015
47739.88804	0.171	14.180	0.025	0.747	0.072	0.407	0.028	—	—
47740.92513	0.233	14.272	0.016	0.766	0.040	0.415	0.020	0.847	0.021
47836.64811	0.950	14.737	0.015	0.785	0.023	0.444	0.017	0.847	0.022
47839.55145	0.123	14.085	0.019	0.533	0.021	0.340	0.017	0.639	0.030
47839.80630	0.139	14.134	0.018	0.606	0.021	0.368	0.019	0.688	0.024
47840.64168	0.189	14.220	0.017	0.664	0.023	0.398	0.019	0.763	0.035
47840.81043	0.199	14.200	0.015	0.703	0.020	0.420	0.025	0.750	0.020
47841.58261	0.245	14.251	0.022	0.737	0.024	0.421	0.034	0.795	0.031
47842.58882	0.305	14.388	0.017	0.858	0.023	0.484	0.021	0.862	0.015
47843.60892	0.366	14.519	0.031	0.959	0.023	0.494	0.030	0.924	0.022
47844.81720	0.438	14.623	0.043	0.971	0.034	0.515	0.028	0.997	0.033
47845.58522	0.484	14.766	0.019	1.036	0.022	0.585	0.024	1.001	0.023
47845.80466	0.497	14.719	0.029	0.996	0.036	0.513	0.032	0.991	0.031
49348.61534	0.259	14.303	0.006	0.779	0.009	0.424	0.010	0.809	0.013
49348.62159	0.260	14.334	0.007	0.758	0.009	0.439	0.010	0.822	0.013
49349.56601	0.316	14.386	0.008	0.841	0.011	0.456	0.013	0.869	0.014
49349.63476	0.320	14.405	0.007	0.844	0.009	0.473	0.010	0.867	0.011
49350.56043	0.376	14.483	0.007	0.897	0.009	0.487	0.009	0.909	0.011
49350.63751	0.380	14.485	0.014	0.896	0.017	0.487	0.017	0.923	0.017
49351.57082	0.436	14.562	0.008	0.972	0.011	0.505	0.010	0.944	0.013
49351.61666	0.439	14.571	0.012	0.945	0.014	0.512	0.016	0.949	0.017
49353.57842	0.556	14.782	0.013	1.039	0.016	0.574	0.019	1.030	0.022
49355.58116	0.675	14.994	0.009	1.071	0.012	0.571	0.013	1.058	0.015
49355.65060	0.680	14.970	0.008	1.074	0.011	0.547	0.010	1.025	0.013
50113.56660	0.950	14.713	0.010	0.786	0.015	0.450	0.013	0.799	0.019
50294.86939	0.779	14.948	0.022	1.002	0.021	0.495	0.018	1.005	0.019
50351.76298	0.177	14.203	0.008	0.671	0.013	0.389	0.012	0.726	0.013
50351.88174	0.184	14.202	0.013	0.681	0.019	0.400	0.013	0.708	0.025
50352.82003	0.240	14.260	0.013	0.771	0.022	0.414	0.018	0.776	0.028
50353.77205	0.297	14.330	0.010	0.849	0.014	0.454	0.015	0.856	0.018
50353.82572	0.300	14.346	0.010	0.839	0.013	0.445	0.013	0.875	0.016
50354.78105	0.357	14.434	0.008	0.892	0.012	0.494	0.010	0.888	0.017
50354.88527	0.364	14.457	0.012	0.907	0.017	0.483	0.016	0.876	0.026
50357.86083	0.541	14.741	0.015	1.007	0.020	0.545	0.019	1.026	0.028
50358.82613	0.599	14.846	0.010	1.069	0.015	0.562	0.016	1.014	0.017
50359.84048	0.659	14.969	0.009	1.064	0.013	0.555	0.011	1.047	0.013

Table 11. Photometric values for HV 1328.

HJD - 2400000. days	Phase	V mag	σ_V mag	$(B - V)$ mag	$\sigma_{(B-V)}$ mag	$(V - R)$ mag	$\sigma_{(V-R)}$ mag	$(V - I)$ mag	$\sigma_{(V-I)}$ mag
47487.56801	0.055	13.837	0.027	0.382	0.039	0.324	0.030	—	—
47488.54714	0.117	13.969	0.034	0.444	0.041	0.355	0.034	0.648	0.041
47489.55266	0.180	13.971	0.032	0.543	0.029	0.348	0.019	0.653	0.024
47490.58392	0.245	14.072	0.030	0.577	0.024	0.395	0.017	0.703	0.024
47491.53388	0.305	14.101	0.035	0.719	0.046	0.408	0.052	0.696	0.031
47492.60051	0.373	14.217	0.039	—	—	—	—	0.798	0.093
47492.61139	0.373	14.209	0.039	—	—	—	—	0.825	0.087
47493.63727	0.438	14.328	0.023	0.737	0.028	0.417	0.031	0.762	0.026
47494.59140	0.498	14.416	0.014	0.703	0.021	0.438	0.019	0.778	0.026
47495.54287	0.558	14.455	0.017	0.748	0.022	0.415	0.022	0.797	0.029
47496.61575	0.626	14.445	0.015	0.706	0.023	0.411	0.021	0.824	0.018
47738.92945	0.928	13.872	0.015	0.390	0.017	0.309	0.017	0.564	0.015
47739.85656	0.986	13.750	0.045	0.414	0.054	0.295	0.026	0.572	0.035
47740.92045	0.053	13.820	0.029	0.406	0.049	0.340	0.031	0.621	0.062
47836.59927	0.095	13.840	0.040	0.453	0.074	0.325	0.032	0.591	0.057
47837.85425	0.174	13.990	0.077	0.365	0.070	0.322	0.051	0.504	0.093
47838.77851	0.233	13.937	0.069	0.623	0.113	0.374	0.064	0.632	0.102
47839.51789	0.279	14.009	0.062	0.564	0.073	0.383	0.085	0.672	0.081
47840.61940	0.349	14.135	0.037	0.593	0.038	0.388	0.028	0.739	0.045
47840.79023	0.360	14.138	0.045	0.607	0.041	0.398	0.043	0.712	0.055
47841.56381	0.409	14.318	0.023	0.637	0.041	0.400	0.037	0.765	0.043
47841.77508	0.422	14.160	0.099	0.621	0.066	0.413	0.066	0.744	0.100
47842.55560	0.471	14.272	0.051	0.633	0.036	0.412	0.028	0.778	0.040
49348.56667	0.572	14.447	0.011	0.687	0.032	0.423	0.020	0.771	0.021
49348.57292	0.572	14.475	0.007	0.711	0.010	0.452	0.010	0.818	0.009
49349.54512	0.634	14.457	0.008	0.694	0.013	0.416	0.013	0.787	0.016
49349.61525	0.638	14.473	0.009	0.670	0.011	0.403	0.016	0.771	0.017
49349.65970	0.641	14.488	0.013	0.666	0.014	0.416	0.014	0.783	0.019
49350.54093	0.696	14.393	0.008	0.633	0.012	0.410	0.014	0.751	0.015
49350.61801	0.701	14.388	0.008	0.590	0.019	0.399	0.014	0.753	0.015
49350.65620	0.704	14.344	0.064	0.594	0.027	0.412	0.015	0.735	0.020
49351.55062	0.760	14.305	0.008	0.550	0.014	0.387	0.013	0.716	0.013
49351.59715	0.763	14.296	0.008	0.563	0.014	0.385	0.014	0.692	0.013
49352.54921	0.823	14.243	0.007	0.531	0.012	0.361	0.012	0.676	0.010
49352.62768	0.828	14.234	0.011	0.503	0.016	0.374	0.013	0.687	0.016
49353.55683	0.887	14.047	0.008	0.484	0.013	0.321	0.013	0.612	0.015
49353.63114	0.892	14.046	0.008	0.445	0.012	0.343	0.012	0.624	0.013
49354.56167	0.950	13.797	0.008	0.372	0.011	0.278	0.011	0.543	0.010
49354.64986	0.956	13.788	0.008	0.381	0.010	0.277	0.011	0.526	0.017
49355.55957	0.013	13.750	0.008	0.358	0.011	0.280	0.010	0.527	0.010
49355.63109	0.018	13.751	0.010	0.381	0.011	0.238	0.012	0.516	0.013
50113.54439	0.878	14.057	0.041	0.487	0.032	0.345	0.031	0.661	0.033
50114.58190	0.944	13.808	0.012	0.382	0.014	0.299	0.016	0.584	0.027
50115.53813	0.004	13.725	0.010	0.360	0.014	0.293	0.014	0.560	0.019
50289.79112	0.008	13.684	0.011	0.356	0.013	0.277	0.014	0.547	0.019
50293.90775	0.267	14.032	0.037	0.598	0.028	0.342	0.033	0.736	0.034
50294.88634	0.329	14.135	0.036	0.633	0.022	0.404	0.027	0.779	0.027
50351.80396	0.923	13.870	0.033	0.407	0.018	0.354	0.016	0.597	0.036
50352.79629	0.986	13.748	0.049	0.346	0.045	0.308	0.018	0.572	0.035
50353.74208	0.046	13.780	0.015	0.382	0.018	0.316	0.017	0.585	0.019
50353.79143	0.049	13.781	0.013	0.381	0.018	0.326	0.016	0.611	0.020
50353.87713	0.054	13.788	0.015	0.419	0.020	0.298	0.016	0.583	0.023
50354.74764	0.109	13.897	0.011	0.457	0.015	0.341	0.010	0.637	0.016
50354.79667	0.112	13.898	0.013	0.471	0.014	0.351	0.014	0.638	0.018
50354.89968	0.119	13.936	0.031	0.475	0.021	0.352	0.016	0.648	0.038
50357.81655	0.303	14.158	0.019	0.608	0.036	0.386	0.026	0.741	0.031
50358.84852	0.368	14.262	0.013	0.649	0.017	0.407	0.016	0.789	0.020

Table 12. Photometric values for HV 1333.

HJD - 2400000. days	Phase	V mag	σ_V mag	(B − V) mag	$\sigma_{(B-V)}$ mag	(V − R) mag	$\sigma_{(V-R)}$ mag	(V − I) mag	$\sigma_{(V-I)}$ mag
47487.58486	0.772	15.067	0.015	0.868	0.033	0.475	0.027	0.977	0.022
47489.57384	0.894	15.022	0.014	0.799	0.036	0.414	0.024	0.872	0.040
47490.59735	0.957	14.401	0.011	0.464	0.031	0.345	0.020	0.675	0.025
47491.66814	0.023	14.296	0.014	0.481	0.027	0.324	0.018	0.659	0.021
47492.64935	0.083	14.379	0.019	0.514	0.036	0.391	0.022	0.735	0.031
47493.67709	0.146	14.443	0.012	0.661	0.024	0.375	0.018	0.766	0.019
47494.61802	0.204	14.494	0.012	0.694	0.024	0.368	0.016	0.804	0.018
47496.64144	0.328	14.676	0.016	0.616	0.028	0.450	0.021	0.911	0.023
47737.91330	0.136	14.457	0.008	0.604	0.056	—	—	—	—
47738.88472	0.195	14.489	0.012	0.689	0.071	0.407	0.031	0.792	0.050
47739.91306	0.258	14.502	0.015	0.782	0.047	0.423	0.026	0.878	0.031
47740.90853	0.320	14.619	0.019	0.847	0.060	0.485	0.027	0.934	0.035
47836.55777	0.190	14.445	0.011	0.664	0.032	0.439	0.020	0.752	0.027
47837.81813	0.267	14.565	0.007	0.695	0.028	0.443	0.017	0.824	0.027
47838.50769	0.310	14.590	0.022	0.736	0.060	0.466	0.038	0.864	0.057
47839.52778	0.372	14.694	0.011	0.841	0.048	0.488	0.030	0.929	0.043
47839.77360	0.387	14.686	0.009	0.807	0.038	0.486	0.025	0.886	0.042
47840.60482	0.438	14.851	0.014	0.725	0.044	0.488	0.029	0.912	0.057
47840.77773	0.449	14.799	0.011	0.844	0.033	0.520	0.022	0.910	0.041
47841.55269	0.496	14.830	0.015	0.917	0.053	0.497	0.039	0.934	0.057
47841.75963	0.509	14.887	0.014	0.822	0.095	0.499	0.062	0.966	0.092
47842.78597	0.572	15.049	0.030	0.919	0.059	0.544	0.037	1.021	0.059
47843.56024	0.620	15.064	0.013	0.904	0.057	0.504	0.028	0.970	0.044
47843.76371	0.632	15.048	0.033	0.914	0.074	—	—	—	—
47844.51229	0.678	15.084	0.016	0.892	0.037	0.484	0.024	0.970	0.034
47844.78380	0.695	15.129	0.024	0.832	0.058	0.509	0.021	0.963	0.070
47845.53030	0.741	15.080	0.016	0.870	0.038	0.531	0.024	0.920	0.035
47845.77126	0.755	15.111	0.020	0.768	0.047	0.514	0.032	0.886	0.051
49348.54967	0.987	14.235	0.007	0.442	0.019	0.323	0.013	0.603	0.019
49348.56043	0.988	14.221	0.005	0.452	0.019	0.314	0.012	0.592	0.017
49349.53610	0.048	14.303	0.006	0.517	0.019	0.344	0.012	0.641	0.019
49349.60624	0.052	14.341	0.006	0.505	0.022	0.327	0.014	0.643	0.024
49349.64790	0.055	14.344	0.007	0.521	0.028	0.351	0.016	0.635	0.032
49350.53122	0.109	14.377	0.005	0.588	0.027	0.373	0.015	0.769	0.039
49350.60899	0.114	14.392	0.010	0.589	0.034	0.375	0.023	0.695	0.047
49350.64719	0.116	14.409	0.006	0.592	0.025	0.378	0.017	0.710	0.027
49351.54161	0.171	14.444	0.004	0.643	0.021	0.413	0.012	0.771	0.019
49351.58814	0.174	14.447	0.007	0.674	0.024	0.407	0.015	0.790	0.023
49351.65341	0.178	14.471	0.008	0.655	0.027	0.415	0.019	0.781	0.031
49352.54020	0.232	14.527	0.008	0.711	0.017	0.441	0.011	0.835	0.015
49352.61867	0.237	14.527	0.012	0.720	0.025	0.425	0.018	0.816	0.025
49353.53462	0.293	14.547	0.010	0.802	0.018	0.460	0.028	0.742	0.034
49353.54782	0.294	14.574	0.010	0.795	0.017	0.455	0.014	0.866	0.017
49353.62143	0.298	14.587	0.007	0.787	0.017	0.464	0.017	0.867	0.015
49354.55266	0.356	14.660	0.006	0.824	0.011	0.482	0.013	0.903	0.014
49354.64016	0.361	14.678	0.007	0.848	0.016	0.464	0.013	0.914	0.016
49355.55055	0.417	14.742	0.006	0.891	0.016	0.499	0.010	0.960	0.016
49355.62208	0.421	14.769	0.007	0.881	0.028	0.505	0.017	0.956	0.029
50289.80361	0.756	15.040	0.010	0.843	0.022	0.491	0.016	0.953	0.021
50293.92793	0.009	14.160	0.013	0.500	0.040	—	—	—	—
50294.89944	0.069	14.293	0.013	0.516	0.058	0.292	0.033	0.659	0.055
50351.78589	0.560	15.030	0.008	0.955	0.032	0.531	0.021	0.984	0.033
50351.89750	0.567	15.034	0.010	0.958	0.024	0.513	0.015	1.007	0.024
50352.78370	0.621	15.070	0.008	0.976	0.019	0.528	0.013	0.996	0.016
50353.76158	0.681	15.107	0.011	0.968	0.023	0.515	0.017	0.982	0.022
50353.81493	0.684	15.132	0.011	0.963	0.027	0.556	0.019	1.002	0.029
50354.76979	0.743	15.088	0.009	0.922	0.026	0.483	0.017	0.906	0.029
50354.82075	0.746	15.117	0.010	0.919	0.027	0.476	0.018	0.894	0.029
50357.83577	0.931	14.782	0.011	0.689	0.020	0.400	0.017	0.804	0.020
50358.83757	0.993	14.182	0.011	0.448	0.019	0.314	0.018	0.600	0.018
50359.85192	0.055	14.322	0.009	0.528	0.018	0.342	0.013	0.667	0.015

Table 13. Photometric values for HV 1335.

HJD - 2400000. days	Phase	V mag	σ_V mag	(B − V) mag	$\sigma_{(B−V)}$ mag	(V − R) mag	$\sigma_{(V−R)}$ mag	(V − I) mag	$\sigma_{(V−I)}$ mag
47487.58486	0.844	14.931	0.011	0.610	0.025	0.432	0.017	0.732	0.019
47489.57384	0.983	14.398	0.011	0.444	0.033	0.269	0.020	0.548	0.039
47490.59735	0.054	14.390	0.009	0.464	0.029	0.329	0.017	0.618	0.024
47491.66814	0.128	14.489	0.011	0.563	0.024	0.359	0.016	0.622	0.018
47492.64935	0.197	14.637	0.018	0.594	0.036	0.375	0.023	0.759	0.030
47493.67709	0.268	14.660	0.012	0.696	0.023	0.422	0.015	0.765	0.018
47494.61802	0.333	14.731	0.013	0.743	0.026	0.450	0.015	0.811	0.018
47496.64144	0.474	14.885	0.015	0.749	0.032	0.434	0.022	0.825	0.023
47737.90314	0.250	14.706	0.013	0.723	0.060	0.383	0.034	0.788	0.060
47739.90429	0.389	14.760	0.012	0.774	0.060	0.435	0.028	0.879	0.036
47740.90032	0.458	14.912	0.020	0.802	0.094	0.376	0.056	0.908	0.097
47836.55777	0.110	14.552	0.010	0.483	0.028	0.363	0.021	0.727	0.025
47837.81813	0.197	14.641	0.010	0.586	0.028	0.394	0.019	0.831	0.027
47838.50769	0.245	14.659	0.020	0.649	0.059	0.437	0.037	0.875	0.056
47839.77360	0.333	14.752	0.017	0.804	0.045	0.468	0.034	0.922	0.045
47840.60482	0.391	14.870	0.015	0.802	0.050	0.444	0.032	0.920	0.056
47840.77773	0.403	14.814	0.016	0.824	0.041	0.452	0.026	0.904	0.044
47841.55269	0.457	14.933	0.016	0.808	0.055	0.479	0.039	0.901	0.057
47841.75963	0.471	14.941	0.016	0.767	0.096	0.486	0.062	0.933	0.092
47842.78597	0.543	15.113	0.029	0.848	0.061	0.510	0.037	0.980	0.058
47843.56024	0.597	15.255	0.084	—	—	0.556	0.083	1.059	0.089
47844.51229	0.663	15.003	0.017	0.838	0.038	0.409	0.025	0.914	0.037
47844.78380	0.682	15.201	0.027	0.772	0.061	0.464	0.026	0.945	0.071
47845.53030	0.734	15.137	0.016	0.777	0.039	0.466	0.026	0.895	0.035
47845.77126	0.750	15.132	0.022	0.712	0.050	0.510	0.034	0.922	0.051
49348.54967	0.243	14.653	0.009	0.653	0.020	0.398	0.016	0.787	0.020
49348.56043	0.244	14.649	0.005	0.653	0.019	0.398	0.013	0.785	0.018
49349.53610	0.312	14.727	0.008	0.726	0.020	0.408	0.015	0.809	0.021
49349.60624	0.317	14.718	0.006	0.726	0.022	0.394	0.014	0.810	0.024
49349.64790	0.320	14.730	0.005	0.717	0.028	0.440	0.015	0.828	0.030
49350.53122	0.381	14.831	0.007	0.773	0.029	0.456	0.017	0.847	0.041
49350.60899	0.387	14.823	0.012	0.785	0.036	0.467	0.025	0.859	0.048
49350.64719	0.389	14.825	0.007	0.769	0.025	0.453	0.017	0.867	0.028
49351.54161	0.451	14.927	0.010	0.795	0.024	0.485	0.016	0.897	0.022
49351.58814	0.455	14.950	0.012	0.794	0.027	0.478	0.020	0.893	0.030
49351.65341	0.459	14.915	0.008	0.821	0.028	0.456	0.019	0.890	0.031
49352.54020	0.521	15.007	0.008	0.838	0.018	0.479	0.012	0.916	0.015
49352.61867	0.526	14.983	0.012	0.852	0.025	0.458	0.018	0.907	0.024
49353.53462	0.590	15.116	0.017	0.824	0.025	0.533	0.027	—	—
49353.54782	0.591	15.105	0.016	0.851	0.025	0.478	0.024	0.844	0.030
49353.62143	0.596	15.097	0.009	0.834	0.019	0.485	0.018	0.941	0.016
49354.55266	0.661	15.181	0.014	0.780	0.018	0.530	0.021	0.935	0.020
49354.64016	0.667	15.125	0.008	0.828	0.018	0.468	0.012	0.912	0.018
49355.55055	0.730	15.102	0.007	0.753	0.017	0.460	0.014	0.860	0.025
49355.62208	0.735	15.082	0.006	0.755	0.028	0.382	0.021	0.859	0.029
50293.92793	0.979	14.791	0.013	0.533	0.043	—	—	—	—
50294.89944	0.046	14.377	0.012	0.477	0.058	0.347	0.032	0.607	0.055
50351.78589	0.002	14.445	0.041	0.473	0.089	0.323	0.059	0.549	0.072
50351.89750	0.009	14.305	0.010	0.392	0.022	0.321	0.015	0.428	0.055
50352.78370	0.071	14.438	0.009	0.496	0.019	0.343	0.014	0.674	0.018
50353.76158	0.139	14.582	0.022	0.556	0.038	0.376	0.031	0.799	0.030
50353.81493	0.143	14.550	0.012	0.552	0.026	0.381	0.021	0.772	0.031
50357.83577	0.422	14.889	0.013	0.772	0.022	0.483	0.019	0.865	0.023
50358.83757	0.492	14.979	0.009	0.811	0.019	0.485	0.016	0.911	0.015
50359.85192	0.563	15.064	0.010	0.834	0.017	0.507	0.014	0.922	0.016

Table 14. Photometric values for HV 1345.

HJD - 2400000. days	Phase	V mag	σ_V mag	$(B-V)$ mag	$\sigma_{(B-V)}$ mag	$(V-R)$ mag	$\sigma_{(V-R)}$ mag	$(V-I)$ mag	$\sigma_{(V-I)}$ mag
47487.60924	0.377	14.787	0.022	0.847	0.034	0.405	0.032	0.846	0.039
47488.58073	0.450	14.978	0.036	0.834	0.053	0.472	0.038	0.956	0.085
47489.58555	0.524	15.017	0.021	0.877	0.028	0.462	0.021	0.910	0.030
47490.60981	0.600	15.109	0.018	0.872	0.023	0.485	0.019	0.948	0.026
47492.66181	0.752	15.095	0.054	0.765	0.061	0.426	0.058	—	—
47493.53955	0.817	14.910	0.013	0.701	0.022	0.403	0.024	0.813	0.019
47495.60683	0.971	14.442	0.013	0.497	0.024	0.306	0.015	0.645	0.020
47496.54013	0.040	14.395	0.013	0.485	0.024	0.308	0.019	0.637	0.020
47737.92653	0.949	14.578	0.013	0.574	0.020	0.318	0.017	0.659	0.014
47738.90655	0.022	14.359	0.017	0.537	0.023	0.303	0.017	0.596	0.021
47739.91637	0.097	14.467	0.027	0.637	0.057	0.352	0.023	0.715	0.027
47740.91330	0.171	14.593	0.045	0.725	0.052	0.391	0.026	0.761	0.029
47836.62105	0.272	14.692	0.022	0.738	0.030	0.415	0.018	0.802	0.031
47837.82933	0.361	14.789	0.029	0.776	0.036	0.385	0.039	0.794	0.080
47838.52096	0.413	14.839	0.027	0.686	0.064	0.413	0.030	0.877	0.057
47839.53898	0.488	14.918	0.033	0.906	0.051	0.440	0.041	0.866	0.071
47839.78966	0.507	14.940	0.021	0.856	0.041	0.443	0.025	0.882	0.061
47840.62851	0.569	15.035	0.023	1.064	0.059	0.494	0.034	0.829	0.044
47840.79864	0.582	14.999	0.027	0.865	0.037	0.448	0.035	0.853	0.051
47841.57083	0.639	15.095	0.049	0.854	0.050	—	—	0.855	0.092
47842.56680	0.713	15.042	0.021	0.810	0.024	0.428	0.026	0.863	0.029
47843.60060	0.789	14.916	0.025	0.727	0.034	0.393	0.109	0.765	0.080
49348.59173	0.449	14.928	0.011	0.981	0.032	0.485	0.015	0.898	0.016
49349.55559	0.520	15.001	0.014	0.890	0.019	0.454	0.012	0.926	0.014
49349.62434	0.526	15.009	0.013	0.908	0.015	0.471	0.012	0.917	0.016
49350.55001	0.594	15.096	0.011	0.864	0.017	0.492	0.015	0.941	0.016
49350.62779	0.600	15.093	0.010	0.873	0.019	0.485	0.016	0.910	0.014
49351.56110	0.669	15.079	0.009	0.842	0.018	0.468	0.012	0.897	0.014
49351.60693	0.673	15.075	0.011	0.838	0.017	0.458	0.015	0.878	0.014
49352.55899	0.743	15.005	0.010	0.760	0.013	0.424	0.013	0.805	0.017
49352.63816	0.749	14.985	0.012	0.739	0.015	0.402	0.012	0.832	0.013
49353.56661	0.818	14.867	0.009	0.694	0.015	0.397	0.013	0.774	0.013
49353.64161	0.824	14.891	0.011	0.669	0.014	0.416	0.016	0.806	0.016
49354.57145	0.893	14.860	0.009	0.690	0.013	0.400	0.011	0.751	0.013
49355.56934	0.967	14.402	0.009	0.477	0.012	0.299	0.012	0.600	0.012
49355.64017	0.972	14.391	0.008	0.452	0.009	0.290	0.011	0.598	0.010
50113.55309	0.204	14.580	0.011	0.712	0.019	0.362	0.015	0.751	0.019
50114.59922	0.281	14.667	0.014	0.744	0.020	0.402	0.014	0.839	0.017
50115.55121	0.352	14.749	0.010	0.808	0.016	0.448	0.012	0.848	0.021
50289.98269	0.293	14.679	0.011	0.732	0.017	0.423	0.011	0.868	0.015
50293.93650	0.587	15.073	0.019	0.916	0.027	0.460	0.024	0.891	0.023
50351.81844	0.881	14.890	0.022	0.714	0.021	0.389	0.016	0.841	0.042
50352.77069	0.952	14.436	0.013	0.510	0.016	0.325	0.014	0.648	0.018
50352.83435	0.956	14.524	0.050	0.507	0.029	0.305	0.040	0.593	0.036
50353.75132	0.025	14.348	0.011	0.471	0.014	0.339	0.014	0.642	0.016
50354.75881	0.099	14.471	0.014	0.581	0.015	0.351	0.012	0.702	0.021
50354.80764	0.103	14.490	0.013	0.604	0.016	0.348	0.014	0.650	0.018
50354.86070	0.107	14.575	0.071	0.622	0.025	0.364	0.018	0.704	0.031
50357.84864	0.329	14.725	0.016	0.797	0.019	0.403	0.018	0.858	0.017
50358.85927	0.403	14.865	0.009	0.805	0.014	0.468	0.012	0.903	0.014

Table 15. IR photometry for HV 822

HJD −2400000	Phase	K	$\sigma(K)$	$(J-K)$	$\sigma(J-K)$
50820.54459	0.177	12.529	0.029	0.369	0.033
50821.51467	0.235	12.504	0.004	0.435	0.005
50822.52278	0.295	12.502	0.007	0.427	0.016
50823.51922	0.355	12.455	0.003	0.449	0.004
50824.51542	0.414	12.453	0.005	0.477	0.011
51089.61935	0.249	12.484	0.014	0.452	0.020
51091.56660	0.365	12.465	0.023	0.482	0.033
51092.54709	0.424	12.485	0.022	0.498	0.031
51092.65820	0.430	12.491	0.016	0.482	0.023
51093.56861	0.485	12.489	0.023	0.528	0.033
51093.64631	0.489	12.523	0.014	0.514	0.020
51094.54704	0.543	12.532	0.016	0.555	0.023
51094.63107	0.548	12.568	0.008	0.541	0.011
51174.67654	0.329	12.460	0.005	0.456	0.012
51175.59593	0.384	12.451	0.022	0.497	0.031
51176.59805	0.444	12.461	0.005	0.526	0.006
51183.66462	0.866	12.861	0.018	0.446	0.025
51185.61787	0.983	12.743	0.023	0.349	0.033
51205.56010	0.174	12.534	0.006	0.434	0.007
51206.57404	0.235	12.506	0.004	0.427	0.005
51207.56762	0.294	12.455	0.002	0.456	0.009
51208.57264	0.354	12.453	0.024	0.480	0.034
51566.57520	0.737	12.722	0.026	0.611	0.037
51567.51820	0.794	12.803	0.011	0.565	0.016
51568.53480	0.854	12.841	0.020	0.519	0.028
51569.52550	0.914	12.888	0.012	0.509	0.017

Table 16. IR photometry for HV 1328

HJD −2400000	Phase	K	$\sigma(K)$	$(J-K)$	$\sigma(J-K)$
50820.55702	0.524	12.593	0.018	0.446	0.023
50821.53085	0.585	12.686	0.047	0.434	0.056
50822.53509	0.649	12.670	0.029	0.469	0.041
50823.53067	0.712	12.692	0.051	0.414	0.061
51089.55144	0.510	12.581	0.042	0.466	0.059
51091.52972	0.635	12.654	0.033	0.457	0.047
51092.50612	0.697	12.668	0.036	0.487	0.051
51092.62417	0.704	12.659	0.036	0.409	0.051
51093.52836	0.761	12.682	0.040	0.431	0.057
51093.61845	0.767	12.733	0.042	0.351	0.059
51094.51286	0.823	12.695	0.044	0.391	0.062
51094.60046	0.829	12.651	0.030	0.378	0.042
51174.63282	0.883	12.632	0.014	0.416	0.015
51175.55282	0.941	12.571	0.029	0.313	0.031
51176.54591	0.004	12.568	0.029	0.255	0.032
51178.54165	0.130	12.527	0.010	0.367	0.012
51180.58887	0.259	12.496	0.014	0.435	0.018
51183.59299	0.449	12.541	0.041	0.479	0.058
51185.55519	0.573	12.670	0.052	0.442	0.074
51204.57956	0.774	12.683	0.024	0.396	0.029
51205.52678	0.834	12.661	0.007	0.398	0.018
51206.53025	0.897	12.599	0.014	0.390	0.019
51207.53372	0.960	12.498	0.034	0.370	0.048
51208.53233	0.024	12.510	0.020	0.287	0.026

Table 17. IR photometry for HV 1333

HJD −2400000	Phase	K	$\sigma(K)$	$(J-K)$	$\sigma(J-K)$
50821.53906	0.391	12.670	0.002	0.525	0.005
50822.54378	0.452	12.691	0.026	0.528	0.026
50823.53940	0.513	12.744	0.012	0.534	0.023
50824.53650	0.575	12.836	0.017	0.532	0.022
51091.54086	0.962	12.927	0.021	0.341	0.030
51092.52414	0.022	12.822	0.054	0.295	0.076
51092.63108	0.029	12.845	0.019	0.270	0.027
51093.54079	0.085	12.797	0.017	9.999	9.999
51093.62551	0.090	12.783	0.021	0.366	0.030
51094.52061	0.145	12.725	0.013	0.391	0.018
51094.61025	0.150	12.742	0.055	0.378	0.078
51174.64533	0.062	12.773	0.012	0.382	0.040
51175.56192	0.119	12.757	0.011	0.400	0.013
51176.56321	0.180	12.704	0.011	0.422	0.030
51178.55004	0.302	12.661	0.008	0.480	0.010
51180.60417	0.428	12.676	0.019	0.597	0.045
51183.60973	0.612	12.828	0.017	0.553	0.024
51184.59200	0.673	12.900	0.024	0.520	0.034
51204.59486	0.900	13.002	0.021	0.502	0.030
51206.53930	0.020	12.778	0.012	0.359	0.018
51207.54277	0.081	12.788	0.015	0.408	0.048

Table 18. IR photometry for HV 1335

HJD −2400000	Phase	K	$\sigma(K)$	$(J-K)$	$\sigma(J-K)$
50821.54829	0.666	13.032	0.024	0.483	0.027
50822.55359	0.736	13.205	0.087	0.321	0.123
50823.54960	0.805	13.222	0.020	0.350	0.028
50824.54488	0.874	13.051	0.032	0.504	0.043
51089.57911	0.303	12.895	0.056	0.346	0.079
51091.54857	0.440	12.874	0.034	0.467	0.048
51092.53111	0.508	12.927	0.015	0.458	0.021
51092.63738	0.516	12.884	0.055	0.516	0.078
51093.55166	0.579	13.017	0.076	0.455	0.107
51093.63177	0.585	13.084	0.051	0.369	0.072
51094.53171	0.647	13.093	0.035	0.417	0.049
51094.61775	0.653	13.089	0.085	0.429	0.120
51174.65707	0.219	12.856	0.060	0.425	0.085
51175.57443	0.282	12.844	0.030	0.402	0.030
51176.57860	0.352	12.837	0.065	0.405	0.092
51178.56675	0.491	12.907	0.040	0.449	0.052
51183.62818	0.842	13.134	0.033	0.430	0.047
51184.60451	0.910	13.093	0.014	0.410	0.020
51204.60181	0.301	12.872	0.059	0.384	0.059
51205.54625	0.367	12.822	0.075	0.437	0.106
51206.55111	0.436	12.867	0.022	0.451	0.028
51207.55181	0.506	12.898	0.019	0.483	0.033
51208.54972	0.575	13.007	0.049	0.448	0.051

Table 19. IR photometry for HV 1345

HJD −2400000	Phase	K	$\sigma(K)$	$(J-K)$	$\sigma(J-K)$
50820.58937	0.661	12.891	0.025	0.557	0.054
50821.55653	0.732	12.927	0.014	0.579	0.015
50822.56058	0.807	12.984	0.006	0.506	0.011
50823.55734	0.881	13.015	0.009	0.482	0.012
50824.55426	0.955	12.895	0.011	0.423	0.013
51089.60282	0.619	12.874	0.016	0.546	0.023
51091.55691	0.764	13.018	0.022	0.482	0.031
51092.53885	0.837	12.981	0.027	0.490	0.038
51092.64998	0.845	13.031	0.023	0.448	0.033
51093.56071	0.913	12.949	0.022	0.464	0.031
51093.63928	0.919	12.956	0.026	0.439	0.037
51094.53946	0.986	12.832	0.020	0.372	0.028
51094.62488	0.992	12.846	0.018	0.336	0.025
51174.66597	0.930	12.927	0.010	0.479	0.017
51175.58481	0.999	12.866	0.011	0.403	0.013
51176.58696	0.073	12.826	0.005	0.419	0.006
51178.57490	0.220	12.737	0.005	0.513	0.021
51183.64428	0.597	12.880	0.015	0.537	0.021
51184.62009	0.669	12.913	0.020	0.548	0.028
51185.60139	0.742	12.960	0.023	0.494	0.033
51205.55181	0.222	12.726	0.014	0.503	0.015
51206.56430	0.297	12.698	0.012	0.532	0.013
51207.56083	0.371	12.721	0.003	0.542	0.004
51208.56083	0.445	12.757	0.003	0.539	0.010
51568.57880	0.156	12.762	0.011	0.486	0.016
51569.54940	0.228	12.776	0.011	0.472	0.016

Table 20. The V and $(V-K)$ color curves for HV 822. The $(V-K)$ color has been determined on the basis of the observed V data and the fourier fit to the K-band data.

Phase	V mag	$\sigma(V)$ mag	$(V-K)$ mag	$\sigma(V-K)$ mag	Phase	V mag	$\sigma(V)$ mag	$(V-K)$ mag	$\sigma(V-K)$ mag	Phase	V mag	$\sigma(V)$ mag	$(V-K)$ mag	$\sigma(V-K)$ mag
0.002	13.892	0.007	1.128	0.012	0.274	14.313	0.007	1.836	0.012	0.504	14.693	0.006	2.177	0.012
0.036	14.010	0.008	1.311	0.013	0.282	14.418	0.022	1.946	0.024	0.522	14.775	0.023	2.243	0.025
0.054	14.077	0.007	1.393	0.012	0.297	14.330	0.010	1.868	0.014	0.539	14.721	0.010	2.173	0.014
0.075	14.097	0.011	1.444	0.015	0.300	14.346	0.010	1.884	0.014	0.541	14.741	0.015	2.193	0.018
0.103	14.158	0.023	1.545	0.025	0.305	14.388	0.017	1.926	0.020	0.556	14.782	0.013	2.218	0.016
0.113	14.171	0.012	1.570	0.016	0.309	14.368	0.007	1.910	0.012	0.582	14.807	0.022	2.228	0.024
0.118	14.140	0.008	1.550	0.013	0.316	14.386	0.008	1.932	0.013	0.599	14.846	0.010	2.253	0.014
0.123	14.085	0.019	1.495	0.021	0.318	14.382	0.008	1.928	0.013	0.636	14.931	0.007	2.307	0.012
0.139	14.134	0.018	1.565	0.021	0.320	14.405	0.007	1.951	0.012	0.638	14.942	0.017	2.318	0.020
0.141	14.160	0.006	1.591	0.012	0.342	14.541	0.026	2.092	0.028	0.659	14.969	0.009	2.327	0.013
0.171	14.180	0.025	1.637	0.027	0.357	14.434	0.008	1.988	0.013	0.675	14.994	0.009	2.333	0.013
0.177	14.203	0.008	1.668	0.013	0.363	14.457	0.012	2.011	0.016	0.680	14.970	0.008	2.309	0.013
0.184	14.202	0.013	1.667	0.016	0.366	14.519	0.031	2.073	0.033	0.688	14.986	0.010	2.314	0.014
0.189	14.220	0.017	1.692	0.020	0.376	14.483	0.007	2.036	0.012	0.690	14.954	0.008	2.282	0.013
0.192	14.230	0.008	1.702	0.013	0.380	14.485	0.014	2.038	0.017	0.779	14.948	0.022	2.159	0.024
0.196	14.239	0.013	1.718	0.016	0.393	14.498	0.010	2.049	0.014	0.796	14.954	0.006	2.139	0.012
0.199	14.200	0.015	1.679	0.018	0.396	14.526	0.016	2.074	0.019	0.847	14.815	0.008	1.952	0.013
0.221	14.309	0.020	1.802	0.022	0.436	14.562	0.008	2.091	0.013	0.904	14.850	0.010	1.978	0.014
0.233	14.272	0.016	1.771	0.019	0.438	14.623	0.043	2.152	0.044	0.926	14.877	0.008	2.022	0.013
0.238	14.274	0.006	1.779	0.012	0.439	14.571	0.012	2.100	0.016	0.929	14.895	0.012	2.040	0.016
0.240	14.272	0.011	1.777	0.015	0.443	14.578	0.006	2.107	0.012	0.942	14.791	0.010	1.945	0.014
0.240	14.260	0.013	1.765	0.016	0.460	14.693	0.036	2.208	0.037	0.950	14.713	0.010	1.878	0.014
0.245	14.251	0.022	1.756	0.024	0.465	14.636	0.008	2.151	0.013	0.950	14.737	0.015	1.902	0.018
0.259	14.303	0.006	1.820	0.012	0.484	14.766	0.019	2.266	0.021					
0.260	14.334	0.007	1.851	0.012	0.497	14.719	0.029	2.203	0.031					

Table 21. The V and $(V-K)$ color curves for HV 1328. The $(V-K)$ color has been determined on the basis of the observed V data and the fourier fit to the K-band data.

Phase	V mag	$\sigma(V)$ mag	$(V-K)$ mag	$\sigma(V-K)$ mag	Phase	V mag	$\sigma(V)$ mag	$(V-K)$ mag	$\sigma(V-K)$ mag	Phase	V mag	$\sigma(V)$ mag	$(V-K)$ mag	$\sigma(V-K)$ mag
0.004	13.725	0.010	1.198	0.014	0.280	14.009	0.062	1.518	0.063	0.638	14.473	0.009	1.811	0.013
0.007	13.684	0.011	1.161	0.015	0.303	14.158	0.019	1.673	0.021	0.641	14.488	0.013	1.826	0.016
0.013	13.750	0.008	1.227	0.013	0.305	14.101	0.035	1.618	0.036	0.696	14.393	0.008	1.711	0.013
0.018	13.751	0.010	1.230	0.014	0.329	14.135	0.036	1.653	0.037	0.701	14.388	0.008	1.706	0.013
0.046	13.780	0.015	1.262	0.018	0.349	14.135	0.037	1.652	0.038	0.704	14.344	0.064	1.662	0.065
0.049	13.781	0.013	1.263	0.016	0.360	14.138	0.045	1.652	0.046	0.760	14.305	0.008	1.616	0.013
0.053	13.820	0.029	1.302	0.031	0.368	14.262	0.013	1.773	0.016	0.763	14.296	0.008	1.607	0.013
0.054	13.788	0.015	1.270	0.018	0.373	14.217	0.039	1.728	0.040	0.823	14.243	0.007	1.573	0.012
0.055	13.837	0.027	1.319	0.029	0.373	14.209	0.039	1.720	0.040	0.828	14.234	0.011	1.570	0.015
0.095	13.840	0.040	1.317	0.041	0.409	14.318	0.023	1.808	0.025	0.878	14.057	0.041	1.434	0.042
0.109	13.897	0.011	1.373	0.015	0.422	14.160	0.099	1.643	0.100	0.887	14.047	0.008	1.434	0.013
0.112	13.898	0.013	1.374	0.016	0.438	14.328	0.023	1.796	0.025	0.892	14.046	0.008	1.433	0.013
0.117	13.969	0.034	1.444	0.035	0.471	14.272	0.051	1.715	0.052	0.923	13.870	0.033	1.286	0.034
0.119	13.936	0.031	1.411	0.033	0.498	14.416	0.014	1.834	0.017	0.928	13.872	0.015	1.297	0.018
0.174	13.990	0.077	1.464	0.078	0.558	14.455	0.017	1.831	0.020	0.944	13.808	0.012	1.242	0.016
0.180	13.971	0.032	1.447	0.034	0.572	14.447	0.011	1.817	0.015	0.950	13.797	0.008	1.239	0.013
0.233	13.937	0.069	1.427	0.070	0.572	14.475	0.007	1.845	0.012	0.956	13.788	0.008	1.238	0.013
0.245	14.072	0.030	1.570	0.032	0.626	14.445	0.015	1.787	0.018	0.986	13.748	0.049	1.217	0.050
0.268	14.032	0.037	1.538	0.038	0.634	14.457	0.008	1.799	0.013	0.986	13.750	0.045	1.219	0.046

Table 22. The V and $(V - K)$ color curves for HV 1333. The $(V - K)$ color has been determined on the basis of the observed V data and the fourier fit to the K-band data.

Phase	V mag	$\sigma(V)$ mag	$(V-K)$ mag	$\sigma(V-K)$ mag	Phase	V mag	$\sigma(V)$ mag	$(V-K)$ mag	$\sigma(V-K)$ mag	Phase	V mag	$\sigma(V)$ mag	$(V-K)$ mag	$\sigma(V-K)$ mag
0.009	14.160	0.013	1.330	0.016	0.237	14.527	0.012	1.842	0.016	0.572	15.049	0.030	2.252	0.032
0.023	14.296	0.014	1.478	0.017	0.258	14.502	0.015	1.827	0.018	0.620	15.064	0.013	2.217	0.016
0.048	14.303	0.006	1.515	0.012	0.267	14.565	0.007	1.895	0.012	0.621	15.070	0.008	2.223	0.013
0.052	14.341	0.006	1.553	0.012	0.293	14.547	0.010	1.884	0.014	0.632	15.048	0.033	2.190	0.034
0.055	14.344	0.007	1.556	0.012	0.294	14.574	0.010	1.911	0.014	0.678	15.084	0.016	2.159	0.019
0.055	14.322	0.009	1.534	0.013	0.298	14.587	0.007	1.927	0.012	0.681	15.107	0.011	2.182	0.015
0.069	14.293	0.013	1.521	0.016	0.310	14.590	0.022	1.933	0.024	0.684	15.132	0.011	2.207	0.015
0.083	14.379	0.019	1.613	0.021	0.320	14.619	0.019	1.963	0.021	0.695	15.129	0.024	2.190	0.026
0.109	14.377	0.005	1.628	0.011	0.328	14.676	0.016	2.021	0.019	0.741	15.080	0.016	2.073	0.019
0.114	14.392	0.010	1.643	0.014	0.356	14.660	0.006	2.001	0.012	0.743	15.088	0.009	2.081	0.013
0.116	14.409	0.006	1.665	0.012	0.361	14.678	0.007	2.019	0.012	0.746	15.117	0.010	2.098	0.014
0.136	14.457	0.008	1.722	0.013	0.372	14.694	0.011	2.032	0.015	0.755	15.111	0.020	2.082	0.022
0.136	14.457	0.009	1.722	0.013	0.387	14.686	0.009	2.017	0.013	0.756	15.040	0.010	2.011	0.014
0.146	14.443	0.012	1.712	0.016	0.417	14.742	0.006	2.056	0.012	0.772	15.067	0.015	2.029	0.018
0.171	14.444	0.004	1.722	0.011	0.421	14.769	0.007	2.083	0.012	0.894	15.022	0.014	2.015	0.017
0.174	14.447	0.007	1.725	0.012	0.438	14.851	0.014	2.152	0.017	0.931	14.782	0.011	1.833	0.015
0.178	14.471	0.008	1.754	0.013	0.449	14.799	0.011	2.093	0.015	0.957	14.401	0.011	1.500	0.015
0.190	14.445	0.011	1.733	0.015	0.496	14.830	0.015	2.088	0.018	0.987	14.235	0.007	1.379	0.012
0.195	14.489	0.012	1.783	0.016	0.509	14.887	0.014	2.137	0.017	0.988	14.221	0.005	1.365	0.011
0.204	14.494	0.012	1.788	0.016	0.560	15.030	0.008	2.242	0.013	0.993	14.182	0.011	1.326	0.015
0.232	14.527	0.008	1.837	0.013	0.567	15.034	0.010	2.237	0.014					

Table 23. The V and $(V - K)$ color curves for HV 1335. The $(V - K)$ color has been determined on the basis of the observed V data and the fourier fit to the K-band data.

Phase	V mag	$\sigma(V)$ mag	$(V-K)$ mag	$\sigma(V-K)$ mag	Phase	V mag	$\sigma(V)$ mag	$(V-K)$ mag	$\sigma(V-K)$ mag	Phase	V mag	$\sigma(V)$ mag	$(V-K)$ mag	$\sigma(V-K)$ mag
0.002	14.445	0.041	1.492	0.042	0.312	14.727	0.008	1.883	0.013	0.596	15.097	0.009	2.093	0.013
0.002	14.319	0.015	1.366	0.018	0.317	14.718	0.006	1.876	0.012	0.597	15.255	0.084	2.251	0.085
0.004	14.405	0.010	1.452	0.014	0.320	14.730	0.005	1.888	0.011	0.598	15.155	0.010	2.151	0.014
0.009	14.305	0.010	1.362	0.014	0.322	14.718	0.008	1.876	0.013	0.630	15.170	0.010	2.132	0.014
0.017	14.322	0.013	1.388	0.016	0.333	14.752	0.017	1.912	0.020	0.656	15.135	0.010	2.060	0.014
0.017	14.356	0.010	1.422	0.014	0.333	14.731	0.013	1.891	0.016	0.661	15.181	0.014	2.106	0.017
0.046	14.377	0.012	1.462	0.016	0.362	14.767	0.011	1.927	0.015	0.663	15.003	0.017	1.928	0.020
0.052	14.410	0.018	1.495	0.021	0.380	14.810	0.013	1.967	0.016	0.667	15.125	0.008	2.038	0.013
0.054	14.390	0.009	1.475	0.013	0.381	14.831	0.007	1.988	0.012	0.668	15.086	0.020	1.999	0.022
0.060	14.400	0.014	1.490	0.017	0.387	14.823	0.012	1.977	0.016	0.682	15.201	0.027	2.101	0.029
0.062	14.418	0.007	1.508	0.012	0.389	14.760	0.012	1.914	0.016	0.702	15.170	0.010	2.046	0.014
0.071	14.438	0.009	1.531	0.013	0.389	14.825	0.007	1.979	0.012	0.709	15.190	0.010	2.055	0.014
0.075	14.475	0.010	1.570	0.014	0.391	14.870	0.015	2.024	0.018	0.730	15.102	0.007	1.946	0.012
0.080	14.520	0.010	1.615	0.014	0.403	14.814	0.016	1.965	0.019	0.734	15.137	0.016	1.981	0.019
0.103	14.480	0.018	1.579	0.021	0.418	14.880	0.010	2.021	0.014	0.734	15.210	0.010	2.054	0.014
0.110	14.552	0.010	1.652	0.014	0.422	14.889	0.013	2.030	0.016	0.735	15.060	0.007	1.904	0.012
0.128	14.489	0.011	1.590	0.015	0.436	14.880	0.006	2.010	0.012	0.735	15.082	0.006	1.917	0.012
0.139	14.582	0.022	1.684	0.024	0.452	14.927	0.010	2.051	0.014	0.750	15.132	0.022	1.959	0.024
0.139	14.533	0.010	1.635	0.014	0.455	14.950	0.012	2.074	0.016	0.755	15.018	0.007	1.839	0.012
0.143	14.550	0.012	1.652	0.016	0.457	14.933	0.016	2.050	0.019	0.755	15.006	0.007	1.827	0.012
0.145	14.579	0.018	1.681	0.021	0.458	14.912	0.020	2.029	0.022	0.765	14.985	0.008	1.801	0.013
0.151	14.561	0.010	1.664	0.014	0.459	14.915	0.008	2.032	0.013	0.766	15.220	0.010	2.036	0.014
0.163	14.601	0.017	1.705	0.020	0.463	14.918	0.017	2.035	0.020	0.771	15.058	0.010	1.874	0.014
0.189	14.595	0.008	1.705	0.013	0.471	14.941	0.016	2.051	0.019	0.776	15.086	0.010	1.898	0.014
0.197	14.637	0.018	1.750	0.021	0.474	14.885	0.015	1.995	0.018	0.783	14.974	0.014	1.786	0.017
0.197	14.641	0.010	1.754	0.014	0.487	14.970	0.010	2.065	0.014	0.785	14.965	0.008	1.776	0.013
0.239	14.765	0.010	1.893	0.014	0.492	14.979	0.009	2.074	0.013	0.798	15.040	0.010	1.851	0.014
0.243	14.653	0.009	1.781	0.013	0.516	15.085	0.010	2.156	0.014	0.823	14.935	0.013	1.751	0.016
0.244	14.649	0.005	1.777	0.011	0.518	14.968	0.017	2.039	0.020	0.827	14.919	0.010	1.741	0.014
0.245	14.659	0.020	1.791	0.022	0.521	15.007	0.008	2.078	0.013	0.844	14.931	0.011	1.760	0.015
0.250	14.706	0.013	1.838	0.016	0.526	14.983	0.012	2.046	0.016	0.864	14.954	0.010	1.803	0.014
0.250	14.707	0.013	1.839	0.016	0.530	15.095	0.010	2.158	0.014	0.870	14.934	0.007	1.795	0.012
0.267	14.675	0.013	1.816	0.016	0.543	15.113	0.029	2.167	0.031	0.904	15.038	0.010	1.941	0.014
0.268	14.660	0.012	1.801	0.016	0.547	15.019	0.013	2.064	0.016	0.937	14.920	0.010	1.886	0.014
0.294	14.736	0.010	1.885	0.014	0.563	15.064	0.010	2.100	0.014	0.962	14.446	0.007	1.442	0.012
0.295	14.730	0.010	1.879	0.014	0.587	15.150	0.010	2.157	0.014	0.979	14.791	0.013	1.815	0.016
0.299	14.714	0.011	1.867	0.015	0.590	15.116	0.017	2.123	0.020	0.980	14.351	0.011	1.375	0.015
0.303	14.781	0.010	1.934	0.014	0.591	15.105	0.016	2.112	0.019	0.983	14.398	0.011	1.422	0.015

Table 24. The V and $(V - K)$ color curves for HV 1345. The $(V - K)$ color has been determined on the basis of the observed V data and the fourier fit to the K-band data.

Phase	V	$\sigma(V)$	$(V - K)$	$\sigma(V - K)$	Phase	V	$\sigma(V)$	$(V - K)$	$\sigma(V - K)$	Phase	V	$\sigma(V)$	$(V - K)$	$\sigma(V - K)$
	mag	mag	mag	mag		mag	mag	mag	mag		mag	mag	mag	mag
0.022	14.359	0.017	1.517	0.020	0.408	14.900	0.015	2.164	0.018	0.713	15.042	0.021	2.129	0.023
0.025	14.348	0.011	1.506	0.015	0.413	14.839	0.027	2.103	0.029	0.735	14.997	0.014	2.061	0.017
0.040	14.395	0.013	1.563	0.016	0.441	14.916	0.008	2.162	0.013	0.739	15.003	0.010	2.067	0.014
0.097	14.467	0.027	1.653	0.029	0.449	14.928	0.011	2.167	0.015	0.743	15.005	0.010	2.069	0.014
0.099	14.471	0.014	1.657	0.017	0.450	14.978	0.036	2.217	0.037	0.749	14.985	0.012	2.040	0.016
0.103	14.490	0.013	1.676	0.016	0.471	14.971	0.006	2.193	0.012	0.752	15.095	0.054	2.150	0.055
0.104	14.523	0.008	1.709	0.013	0.488	14.918	0.033	2.121	0.034	0.772	14.939	0.007	1.975	0.012
0.106	14.511	0.008	1.701	0.013	0.507	14.940	0.021	2.123	0.023	0.775	14.923	0.007	1.959	0.012
0.107	14.519	0.010	1.709	0.014	0.520	15.001	0.014	2.174	0.017	0.789	14.916	0.025	1.934	0.027
0.107	14.575	0.071	1.765	0.072	0.524	15.017	0.021	2.190	0.023	0.810	14.886	0.008	1.889	0.013
0.171	14.593	0.045	1.818	0.046	0.525	15.009	0.013	2.173	0.016	0.818	14.910	0.013	1.908	0.016
0.181	14.616	0.013	1.848	0.016	0.552	15.077	0.008	2.223	0.013	0.818	14.867	0.009	1.865	0.013
0.204	14.580	0.011	1.827	0.015	0.553	15.057	0.008	2.203	0.013	0.824	14.891	0.011	1.889	0.015
0.272	14.692	0.022	1.975	0.024	0.569	15.035	0.023	2.167	0.025	0.881	14.890	0.022	1.899	0.024
0.281	14.667	0.014	1.952	0.017	0.582	14.999	0.027	2.125	0.029	0.884	14.876	0.010	1.885	0.014
0.292	14.733	0.008	2.020	0.013	0.587	15.073	0.019	2.195	0.021	0.886	14.878	0.008	1.895	0.013
0.293	14.713	0.013	2.000	0.016	0.592	15.103	0.008	2.225	0.013	0.893	14.860	0.009	1.877	0.013
0.293	14.679	0.011	1.966	0.015	0.593	15.100	0.011	2.222	0.015	0.922	14.712	0.011	1.763	0.015
0.329	14.725	0.016	2.012	0.019	0.594	15.096	0.011	2.218	0.015	0.949	14.578	0.013	1.669	0.016
0.352	14.749	0.010	2.033	0.014	0.600	15.093	0.010	2.211	0.014	0.949	14.604	0.024	1.695	0.026
0.361	14.789	0.029	2.071	0.031	0.600	15.109	0.018	2.227	0.021	0.952	14.436	0.013	1.527	0.016
0.365	14.815	0.011	2.095	0.015	0.616	15.145	0.011	2.257	0.015	0.957	14.524	0.050	1.627	0.051
0.368	14.830	0.006	2.110	0.012	0.639	15.095	0.049	2.204	0.050	0.967	14.402	0.009	1.517	0.013
0.378	14.787	0.022	2.064	0.024	0.669	15.079	0.009	2.182	0.013	0.971	14.442	0.013	1.557	0.016
0.404	14.865	0.009	2.134	0.013	0.673	15.075	0.011	2.178	0.015	0.972	14.391	0.008	1.506	0.013
0.405	14.868	0.013	2.137	0.016	0.699	15.078	0.007	2.170	0.012	0.998	14.332	0.010	1.476	0.014

Table 25. Radial velocities for the SMC Cepheids. Typical errors, including systematics, are 1.5km s^{-1} .

HV 822		HV 1328		HV 1333		HV 1335		HV 1345	
HJD −2400000	Radial velocity km s^{-1}	HJD −2400000	Radial velocity km s^{-1}	HJD −2400000	Radial velocity km s^{-1}	HJD −2400000	Radial velocity km s^{-1}	HJD −2400000	Radial velocity km s^{-1}
47096.5740	127.6	47096.7153	111.5	47097.5649	152.2	47096.6795	172.5	47096.5365	102.0
47097.6649	127.2	47097.6319	114.5	47098.5545	147.5	47098.5906	166.4	47097.5295	109.4
47098.6260	112.0	47098.6558	118.6	47099.5442	142.9	47099.5757	158.2	47098.5191	115.1
47099.6518	109.1	47099.6007	122.2	47100.6159	128.4	47100.6452	154.8	47099.5148	122.0
47100.6868	96.7	47100.5698	123.4	47101.5941	120.8	47100.6573	154.5	47100.5295	124.9
47101.5594	77.6	47101.6921	121.0	47103.5510	126.7	47100.7149	154.5	47101.5243	124.6
47483.7983	111.0	47103.6375	114.4	47483.6458	158.5	47101.6348	138.6	47103.6691	105.6
47484.7722	108.2	47483.5996	114.2	47484.6277	162.0	47101.7302	143.7	47483.7587	96.5
47485.7485	96.8	47484.5902	106.7	47485.6033	166.3	47103.6059	136.4	47484.7242	89.5
47486.7783	75.8	47485.5676	102.4	47486.6352	168.0	47483.6985	170.0	47485.6893	92.9
47840.7635	73.2	47486.5984	100.1	47840.5975	147.5	47484.6756	172.3	47486.7312	99.5
47841.6253	78.8	47840.6899	108.3	47841.7041	153.7	47485.6506	174.0	47840.7285	120.7
47842.5839	84.9	47841.7398	113.7	47842.7103	159.1	47486.6831	158.1	47841.6632	123.8
47843.6283	90.5	47842.7401	117.3	47843.6922	165.2	47840.6489	153.8	47842.6155	124.0
47844.5498	95.6	47843.7220	120.6	47844.6400	169.2	47841.5888	160.1	47842.6503	125.5
47845.5407	101.4	47844.6102	122.8	47845.6330	169.6	47842.6762	162.3	47843.5947	111.4
47846.7508	112.5	47845.6025	121.2	47847.7034	149.7	47843.6588	168.9	47844.5804	104.4
47847.5837	114.0	47847.6712	115.6	47848.7048	144.8	47844.6741	173.9	47845.5720	100.8
47848.5865	119.2	47848.6117	108.3	48913.8374	134.4	47845.6695	171.9	47846.7181	101.0
49675.7149	126.2	48913.7916	103.6	49234.8358	130.5	47847.7416	153.8	49672.6505	113.4
49676.6871	116.0	49234.7401	110.2	49237.6753	123.3	47848.7340	151.7	49676.7225	108.3
49679.5686	84.4	49672.5660	101.3	49237.7169	121.9	49234.6951	148.4		
		49673.5493	102.8	49672.6060	148.6	49237.8329	165.1		
		49674.5354	102.4	49673.5865	145.9	49673.6295	154.5		
		49675.5499	100.6	49674.5625	133.9	49674.5989	153.3		
		49676.5402	106.4	49675.5923	121.0	49676.6020	141.0		
		49677.5540	109.1	49676.5714	120.8	49677.5880	138.1		
		49678.5380	112.8	49677.6221	124.0	49678.5745	136.3		
				49678.6109	128.8	49679.6324	144.2		
				49679.5991	136.5				

Table 26. Radial velocities for the LMC Cepheids.

HV 2694		HV 12198		HV 12797	
HJD −2400000	Radial velocity km s^{-1}	HJD −2400000	Radial velocity km s^{-1}	HJD −2400000	Radial velocity km s^{-1}
47100.7531	295.6	47840.8042	295.0	47100.8337	245.6
47101.7882	256.4	47841.8538	307.7	47483.8379	253.3
49672.8161	281.7	47841.8538	307.8	47484.8240	252.4
49673.7967	294.4	47842.8399	294.0	47485.8042	232.8
49674.7752	266.0	47843.8344	282.8	47486.8247	229.1
49675.7953	255.3	47844.7496	301.5	47840.8470	230.0
49676.7857	264.8	47845.8434	314.5	47841.8206	232.3
49677.7898	271.0	47846.8076	277.5	47842.7949	234.2
49678.7724	277.4	47847.8149	294.9	47843.7945	241.0
49679.8078	287.7	47848.8135	309.9	47844.7098	246.7
		49672.7510	295.9	47845.8053	251.5
		49673.6795	312.2	47846.7799	242.3
		49673.8420	312.7	47847.8507	230.5
		49674.6469	304.0	47848.8577	233.3
		49674.8225	287.5	48913.8813	238.6
		49675.6663	285.5		
		49675.8413	289.4		
		49676.6448	306.4		
		49676.8329	309.3		
		49677.6816	319.8		
		49677.8364	319.5		
		49678.8336	283.1		

Table 27. Radial velocities for two additional stars

ID	HJD −2400000	Radial velocity km s⁻¹
HV 821 (SMC)	47096.6090	100.9
HV 821 (SMC)	47103.6972	105.6
HV 883 (LMC)	47103.7743	243.2